

Review

Recent Insights into Low-Surface-Area Catalysts for Hydrogen Production from Ammonia

Marina Pinzón ¹, Paula Sánchez ¹, Ana Raquel de la Osa ¹, Amaya Romero ²
and Antonio de Lucas-Consuegra ^{1,*}

¹ Department of Chemical Engineering, Faculty of Chemical Sciences and Technologies, University of Castilla-La Mancha, Avenida Camilo José Cela 12, 13071 Ciudad Real, Spain

² Department of Chemical Engineering, Higher Technical School of Agronomical Engineers, University of Castilla-La Mancha, Ronda de Calatrava 7, 13071 Ciudad Real, Spain

* Correspondence: antonio.lconsuegra@uclm.es

Abstract: A potential method of storing and transporting hydrogen safely in a cost-effective and practical way involves the utilization of molecules that contain hydrogen in their structure such as ammonia. Because of its high hydrogen content and carbon-free molecular structure, as well as the maturity of related technology (easy liquefaction), ammonia has gained attention as a “hydrogen carrier” for the generation of energy. Unfortunately, hydrogen production from ammonia requires an efficient catalyst to achieve high conversion at low reaction temperatures. Recently, very attractive results have been obtained with low-surface-area materials. This review paper is focused on summarizing and comparing recent advances in novel, economic and active catalysts for this reaction, paying particular attention to materials with low surface area such as silicon carbide (SiC) and perovskites (ABO₃ structure). The effects of the supports, the active phase and the addition of promoters in such low-porosity materials have been analyzed in detail. Advances in adequate catalytic systems (including support and active metal) benefit the perspective of ammonia as a hydrogen carrier for the decarbonization of the energy sector and accelerate the “hydrogen economy”.

Keywords: hydrogen production; ammonia decomposition; catalysts; low surface area; ruthenium; nickel; cobalt; novel support



Citation: Pinzón, M.; Sánchez, P.; de la Osa, A.R.; Romero, A.; de Lucas-Consuegra, A. Recent Insights into Low-Surface-Area Catalysts for Hydrogen Production from Ammonia. *Energies* **2022**, *15*, 8143. <https://doi.org/10.3390/en15218143>

Academic Editor: Alberto Abánades

Received: 28 September 2022

Accepted: 27 October 2022

Published: 1 November 2022

Publisher's Note: MDPI stays neutral with regard to jurisdictional claims in published maps and institutional affiliations.



Copyright: © 2022 by the authors. Licensee MDPI, Basel, Switzerland. This article is an open access article distributed under the terms and conditions of the Creative Commons Attribution (CC BY) license (<https://creativecommons.org/licenses/by/4.0/>).

1. Introduction

A great deal of effort is made by the scientific community to identify new energy sources and vectors to replace fossil fuels through the decarbonization of the energy sector [1,2]. Despite solar, wind and hydroelectricity technologies being consolidated as renewable energy sources, they suffer intermittency due to weather conditions.

Green hydrogen (H₂), produced from eco-friendly resources, might resolve the problem of the massive energy storage required to mitigate the fluctuations of these energies and meet the global energy demand [3]. The concept of using hydrogen as an energy carrier dates back more than two centuries ago. However, until the energy crisis of the 1970s, its growth was not accentuated. After that, numerous advances were achieved in this field in the 1980s [4].

Hydrogen is a renewable, clean and non-toxic fuel that only releases energy and vapor water into the atmosphere when it is combusted [5]. It does not present spillage problems, as it disperses quickly (due to its very low density), and it has much more chemical energy per mass than any fuel made from hydrocarbons. Its energy content is very high (141.9 MJ kg⁻¹) and very low in volume, showing that it is an adequate carrier of energy. Therefore, hydrogen, instead of being a source of energy, stores energy and delivers it in a usable form, and it is the most abundant element in the universe [6]. Additionally, it yields twice the electricity generation of conventional fossil fuels [7].

In this context, the system that tries to satisfy society's energy needs through hydrogen, instead of using fossil fuels, is known as the "hydrogen economy". The hydrogen economy would provide a lasting response to the triple challenge that the world currently faces: the energy needs of emerging countries, the depletion of fossil resources and the threat of the consequences of climate change [8]. Despite the enormous advantages of establishing this system, its success depends on the development of five key elements: production, delivery, storage, conversion and applications of hydrogen.

Nonetheless, only a small part of the generated H₂ is applied for energy purposes, whereas 92% of H₂ is used as a chemical feedstock and in the metallurgical and petrochemical industries [9].

Currently, 70 Mt_{H₂} per year is demanded (International Energy Agency) by industrial processes, and most H₂ generation relies on methane steam reforming. However, this technique generates about 7 kg of CO₂ per kilogram of H₂ [10] and must be replaced by processes using environmentally friendly routes to reach net zero carbon emission.

However, the success of the hydrogen economy and the use of this compound as an energy carrier depends on the current H₂ storage and transport routes, which are characterized by their high costs (high pressure or low temperature) [11]. A potential solution to this issue involves the utilization of molecules that contain hydrogen in their structure ("H₂ carriers"), which have been explored for storing H₂ safely and in an economically feasible way, so that it is possible to transport it using the current supply networks [12,13].

2. Roles of Ammonia in a Hydrogen Economy

Among the substances capable of assuming the role of H₂ carriers (methane, formic acid, derivatives of amines, ammonia and complex hydrides), ammonia (NH₃) should be highlighted.

The ammonia market involves a mature technology (it is the second most-produced chemical globally) and a relatively low cost of production, storage and distribution using existing rail, road, marine and pipeline networks [14–18]. This compound can be easily liquefied under 8.6 bar and 20 °C, so this procedure consumes less energy than liquid hydrogen (−253 °C at 1 bar), and its vessels and pipes are light and easy to design [19]. In addition, it is a non-flammable, non-dangerous and easily detectable substance. Because of all this, along with the fact that it allows producing 121 kg of H₂ per cubic meter of NH₃, which is double that produced by liquid hydrogen (71 kg of H₂ per cubic meter of liquid H₂), and is a carbon-free molecule, ammonia is considered an excellent H₂ carrier for mitigating issues related to the storage and transport of hydrogen [20,21]. In addition, NH₃ can help in the transition toward a clean future as viable fuel, so it can be directly used thermo-chemically (combustion), in thermal decomposition (ammonia decomposition) and/or electro-chemically (fuel cells), as summarized in Figure 1 [16,19,21–23].

Ammonia is usually produced in large quantities (180 Mt annually) through the catalytic reaction of hydrogen and nitrogen at temperatures around 400–600 °C and pressures around 200–400 atmospheres (Haber-Bosch process). These raw materials come from air and hydrogen separation plants. To reduce the carbon footprint of the Haber-Bosch process, a renewable energy source must be employed. However, the origin of hydrogen can be diverse, ranging from the traditional reforming processes to others that are environmentally friendly (free of CO₂), such as electrolysis [24] or biomass gasification [25]. On the other hand, N₂ could be produced by electrochemical separation processes with high efficiency [26] or by conventional separation processes from the air.

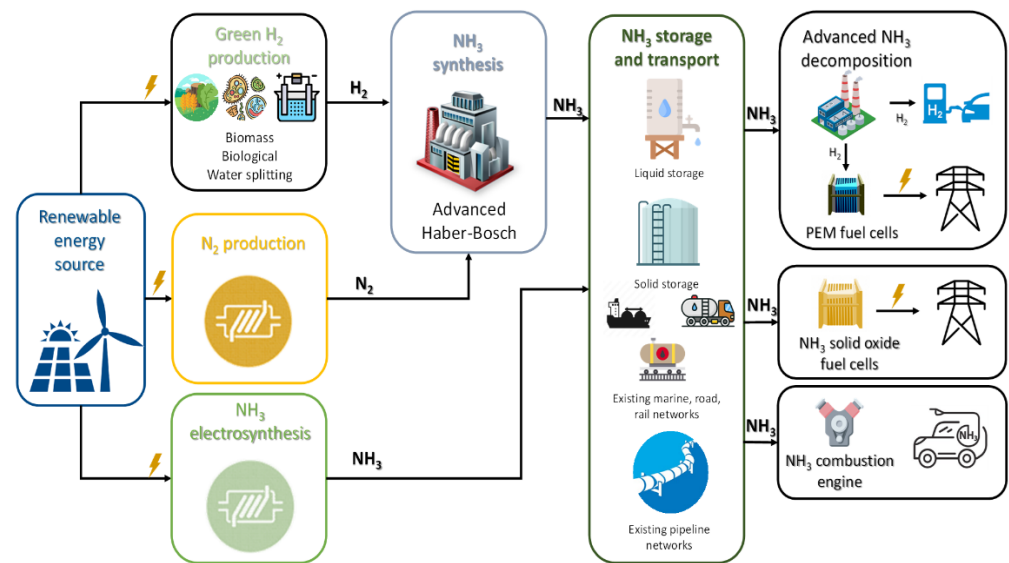


Figure 1. Roles of ammonia in a hydrogen economy. Adapted with permission [22]. Copyright 2021, Elsevier.

On the other hand, there are various review papers focusing on the production of green ammonia to decarbonize the current fossil-fuel-based ammonia industry [18,20,21,27]. Green ammonia production can be carried out through ammonia electrosynthesis [20,27,28]. This method consists in an electrochemical process, where nitrogen is fed to the cathode and hydrogen to the anode in proton-conducting cells. The reactions taking place are as follows:



Electrosynthesis of ammonia consumes about 20% less energy than the Haber–Bosch and is carried out at low temperature and pressure conditions. However, this technology presents a low selectivity and poor maturity.

In recent years, the generalized interest in hydrogen production from ammonia has made it a target in research, as revealed by the increasing number of publications on this topic (Figure 2, from Scopus).

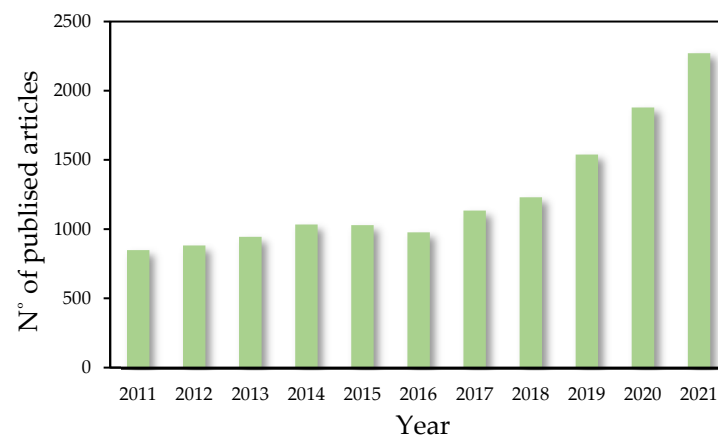


Figure 2. Trend of published articles on the topic of “hydrogen from ammonia” in the last 10 years (source: Scopus, 17 September 2022).

Hydrogen can be produced from ammonia by using various technologies, such as thermal decomposition, microwave, plasma technologies, solar energy and/or ammonia

electrolysis [17]. Among them, the catalytic thermal decomposition of ammonia is the most commonly used method for hydrogen production, owing to its maturity; it can be carried out with or without catalysts and coupled with other parallel exothermic reactions [14].

The key challenges of NH_3 as a carrier of H_2 are the decomposition of ammonia and the separation of H_2 from the reaction products. These processes must be energy-efficient, reliable and scalable to enhance the perspective of ammonia as a hydrogen carrier toward the “hydrogen economy” while fulfilling the requirements of a decarbonized economy, in line with the EU energy policy [29,30].

3. Catalytic Thermal Decomposition of NH_3

Ammonia decomposition using heterogeneous catalysts is extremely interesting because it allows the release of H_2 in a catalytic reactor. The resulting H_2 can be used in situ, either in fuel cells or by direct combustion. Furthermore, this reaction yields H_2 and N_2 as byproducts without carbon (CO_x) emissions. The hydrogen purification can be easily carried out in H_2 -permeable membrane reactors [22]. In this sense, some of the current problems associated with the “hydrogen economy” are avoided, such as its storage and distribution, taking advantage of the benefits related to the use of ammonia.

Most of the investigations that aim to generate H_2 from NH_3 decomposition are performed at elevated temperatures [14,15,31]. However, the application of NH_3 as a hydrogen carrier requires in situ production at suitable reaction conditions (temperatures and pressures) to be used in fuel cells. Therefore, one of the current main challenges is the development of a sufficiently active catalytic system at low temperatures at an affordable cost.

The ammonia decomposition reaction ($\text{NH}_3 \rightleftharpoons \frac{3}{2} \text{H}_2 + \frac{1}{2} \text{N}_2$, $\Delta H^0 = +46 \text{ kJ mol}^{-1}$) is slightly endothermic, and its kinetics depends on two factors: ammonia concentration in the feed and temperature [14]. Many works have been carried out using different active phases and supports to identify the ammonia decomposition mechanism [14,32–34], although the most accepted one includes six steps as suggested by Temkin [14]. It begins with ammonia adsorption in the active sites of the catalyst. Then, the adsorbed NH_3 molecules undergo consecutive N–H bond breaks, releasing hydrogen atoms that combine to form H_2 . The final step involves the desorption and recombination of nitrogen atoms to produce N_2 . This mechanism has been reported to follow six consecutive steps:

- (1) Step 1 : $\text{NH}_3(\text{g}) \rightleftharpoons \text{NH}_3(\text{a})$
- (2) Step 2 : $\text{NH}_3(\text{a}) + \text{s} \rightleftharpoons \text{NH}_2(\text{a}) + \text{H}(\text{a})$
- (3) Step 3 : $\text{NH}_2(\text{a}) + \text{s} \rightleftharpoons \text{NH}(\text{a}) + \text{H}(\text{a})$
- (4) Step 4 : $\text{NH}(\text{a}) + \text{s} \rightleftharpoons \text{N}(\text{a}) + \text{H}(\text{a})$
- (5) Step 5 : $2\text{H}(\text{a}) \rightleftharpoons \text{H}_2(\text{g}) + 2\text{s}$
- (6) Step 6 : $2\text{N}(\text{a}) \rightarrow \text{N}_2(\text{g}) + 2\text{s}$

where s symbolizes a vacant site of the catalyst’s surface, (g) denotes gas and (a) indicates adsorbed molecules. However, two phenomena behave as limiting stages of the reaction regardless of the catalysts: the desorption of nitrogen and the breaking of the N–H bond, and both steps are influenced by the chemical properties of the active metal surface (composition and morphology) as well as the support [14,35].

At high temperatures (between 520 and 690 °C) and high ammonia concentrations (50–780 torr) the ammonia reaction is a first-order reaction concerning ammonia concentration [36]. In the case of working at low temperatures (<400 °C) and high partial pressures of ammonia, a zero-order dependence of the reaction rate on ammonia was observed [14]. Nevertheless, in the high temperature range, both at low ammonia pressure values and feeding pure ammonia, the inhibition by hydrogen did not appear to be significant [36].

Therefore, in any case, the N–M bond strengths (M = active metal surface) are the key in the design of catalysts for ammonia decomposition reaction, and they should be strong enough for the N–H bond scission (or NH_x dehydrogenation steps) to take place but adequately weak to desorb N_2 [32].

Ganley et al. [35] correlated the reaction rate of ammonia decomposition for different metals and the relative rate of N–H bond scission and N–N recombination (estimated

from Blowers–Masel correlation). These authors suggested that the rate-limiting step for ruthenium (Ru), nickel (Ni), cobalt (Co), iron (Fe) and chromium (Cr) catalysts was nitrogen desorption, whereas for rhodium (Rh), iridium (Ir), platinum (Pt), palladium (Pd) and copper (Cu), the limiting step changed, showing a large effect of the active metal surface.

On the other hand, Boisen et al. [37] studied different metals for both the synthesis and decomposition of ammonia, mainly focusing on the rational design of catalysts for the latter. Figure 3 shows the volcano-type correlation between ammonia decomposition rate and nitrogen binding energy. They found that nitrogen binding energies were lower on Ru and Ni with a high $\text{NH}_3:\text{H}_2$ ratio, whereas with a low $\text{NH}_3:\text{H}_2$ ratio, the nitrogen binding energies were stronger, which indicated that the optimal catalysts for ammonia synthesis did not work for its decomposition.

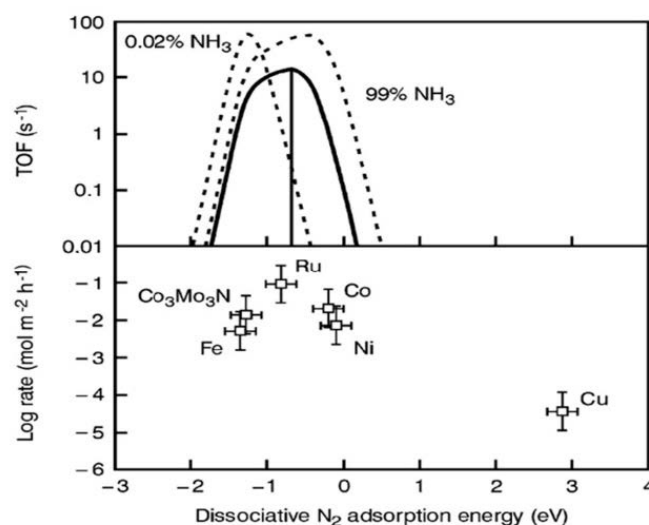


Figure 3. Calculated turnover frequencies of ammonia synthesis/decomposition at 773 K; 1 bar; 3:1 H_2/N_2 ; and 0.02, 20 (solid line) and 99% NH_3 as a function of the reaction energy of dissociative N_2 adsorption. The vertical line gives the dissociative nitrogen binding energy of the optimal ammonia decomposition catalyst when the ammonia concentration is 20%. At these conditions, the gas phase equilibrium NH_3 concentration is 0.13% (top). Experimental rates of ammonia decomposition over various catalysts at 773 K, 1 bar, 3:1 H_2/N_2 and 20% NH_3 (bottom). Reprinted with permission from [37]. Copyright 2005, Elsevier.

Both studies are considered essential references for the design of catalysts based on the rate-determining step for ammonia decomposition. However, there is no general assumption for the rate-determining step, and each catalytic system must be examined in detail [14,34]. Despite this, these studies concluded that Ru is the most active metal phase for the ammonia decomposition reaction.

On the other hand, Lucentini et al. [14] compared the global warming power on a 100-year basis ($\text{kg CO}_2 \text{ kg}^{-1}$) of the elements versus the price of the active metal phase (USD kg^{-1}). As shown in Figure 4, Ru must be avoided due to the high environmental impact related to the use of this element. For that reason, an alternative to Ru is the application of cheaper metals in catalytic supports that enhance ammonia decomposition, also using suitable precursors and optimal operating conditions.

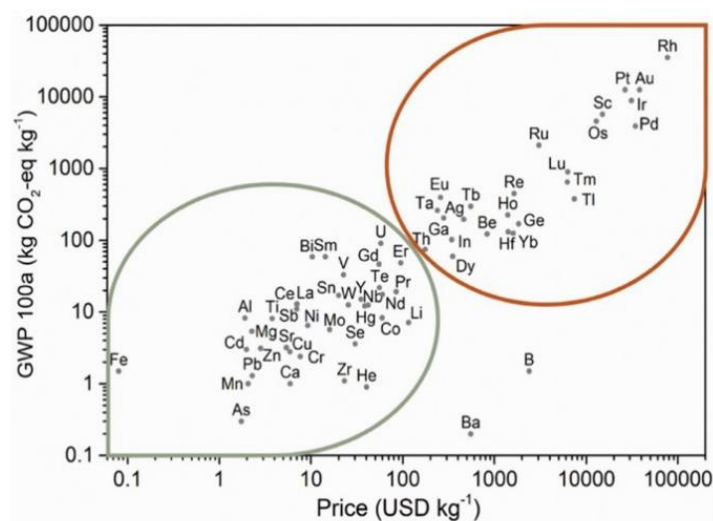


Figure 4. Comparison of the price (USD kg⁻¹) and the global warming power on a 100-year basis (kg CO₂ kg⁻¹) of the elements. Reprinted with permission from [37]. Copyright 2021, ACS.

Apart from all the above, the structure of the catalysts and the configuration of the active site have an important effect on anchoring the ammonia molecule, as well as the existence of vacant sites, to release nitrogen and hydrogen atoms. In fact, the metal crystallite size is essential for catalytic activity since it is a structure-sensitive reaction [38–46]. Overall, a small metal crystallite size leads to a high ammonia conversion and hence a higher hydrogen production.

Ru active sites are made up of crystallites with sizes of around 3–5 nm and are called B5-type sites. This involves one layer of three Ru atoms and two further atoms in the layer directly above [38]. In addition, the shape of the nanoparticles plays a significant role in the generation of these active sites. Indeed, the optimal catalytic activity was found for an elongated-shape crystallite of 7 nm rather than for 2–5 nm crystallites of hemispherical particle shape [39]. The B5-type sites presented a suitable N–M bond strength improving the reaction mechanism.

In the case of non-noble metals, crystallite sizes between 2 and 15 nm maximize the ammonia conversion at low temperatures [45,46]. In particular, nickel size in the range of 3 to 5 nm decreased the energy barrier, and excellent hydrogen production was achieved due to the presence of active sites of B5-type [45]. Moreover, first-principles calculations have shown that the desorption of N took place more easily on Ni(111) [47]. For Co catalysts, Bell et al. [46] suggested that the ammonia conversion was enhanced as the cobalt size diminished, obtaining the maximum activity at 10–20 nm [48].

Considering the promoters, the use of alkaline, alkaline-earth and rare-earth precursors is reported to enhance the catalytic activity due to an increase in the surface area, a reduction in the pore volume and an increase in the electron density of the metals resulting from an increase in the basicity of the catalysts. In addition, it is known that the promoters can decrease the metal size and enhance the stability of the catalyst by hindering the metal agglomeration [42,49–51].

In particular, the use of lanthanum (La) as a promoter results in not only morphological changes of Ni and/or Co active sites but also electronic effects, facilitating recombinant nitrogen desorption and hence increasing the reaction rate. Furthermore, studies show that the use of small amounts of cerium (Ce) greatly reduces the decomposition temperature of ammonia. Zheng et al. [52] estimated an optimum molar ratio of Ce/Ni that allowed the control of the crystallite size of Ni, inhibiting its growth.

The support has a key role in the design of catalysts since it influences their properties. Supports are used to enhance the size, shape and dispersion of the active phase; likewise, they might affect the electronic structure of the metals [53]. Actually, high electron conductivity, basicity, thermal stability and the absence of electron-withdrawing species are

the best requirements for a suitable catalytic support for this reaction [14,48,53]. These properties benefit the electron transfer from the support to the metals, accelerating the desorption of N [32]. Although supports with high surface areas allow the generation of highly dispersed metals with small particle sizes [14], recently, materials with a low surface area, such as silicon carbide (SiC) or perovskite-derived catalysts, have shown an excellent performance in the production of hydrogen from ammonia [40,42–44,54].

In light of this, this review summarizes and compares recent advances in novel, economic and active catalysts for this reaction, paying particular attention to materials with a low surface area ($<35 \text{ m}^2 \text{ g}^{-1}$) such as silicon carbide or perovskites (ABO_3 structure). The effects of the supports, the active metal and the addition of promoters have been analyzed in detail in these non-porous materials.

4. Recent Insights into Low-Surface-Area Catalysts for Catalytic Thermal Decomposition of NH_3

Ruthenium catalysts supported on low-surface-area materials have been widely studied in the literature. These showed the highest catalytic activity at low temperatures. Among the support properties, basicity and conductivity have an important role in enhancing the conversion of ammonia despite the intrinsic low porosity as is seen for rare-earth oxide supports or SiC.

On the one hand, non-noble metals have been also tested in the decomposition of ammonia. Among these, nickel and cobalt are the most studied as active phases of low-surface-area catalysts. The synthesis method and the utilization of precursors, such as perovskites, are key for the generation of a small metal size. Moreover, the addition of promoters improves the activity at low temperatures.

The use of a bimetallic phase or combination of metals is being investigated as a promising alternative in the case of a low-surface-area catalyst. In particular, the $\text{Co}_3\text{Mo}_3\text{N}$ material presents small porosity and high activity.

The recently published catalysts for NH_3 decomposition are classified according to their active phase in Tables 1 and 2. Note that the catalytic activity was evaluated at atmospheric pressure and based on the gas composition feed. However, other experimental factors (support, promoters, gas hourly space velocity, etc.) clearly have an impact on the ammonia conversion. It is important to note that activity decreases with the increase in the gas hourly space velocity and with the increase in the NH_3 inlet flow [14].

4.1. Ruthenium-Based Catalysts

4.1.1. Novel Silicon Carbide Support

As mentioned above, Ru catalysts exhibit excellent catalytic activity. In this sense, our research group has recently investigated for the first time the use of Ru supported on SiC as a catalyst for the ammonia decomposition reaction [40]. Although SiC presented a low specific surface area ($25 \text{ m}^2 \text{ g}^{-1}$), this ceramic material presents interesting properties (i.e., high resistance, chemical inertness, mechanical strength, high thermostability and conductivity). In light of this, a series of Ru/SiC catalysts were synthesized by vacuum impregnation method with different metal loadings (1–5 wt.% of metal). In addition, the calcination conditions (N_2 or air flow, static air or non-calcined) and the reduction temperature (400 °C and 600 °C) were optimized. A maximum catalytic activity (ammonia conversion close to 100% at 350 °C) was obtained at $60,000 \text{ mL-NH}_3/\text{Ar g}_{\text{cat}}^{-1} \text{ h}^{-1}$ for the catalyst containing 2.5 wt.% Ru, calcined in a N_2 atmosphere and reduced at 400 °C. The authors attributed this behavior to the higher proportion of chlorine species (Cl derived from the Ru precursor) removed during the calcination process and the smallest sizes of Ru (5 nm) generated at lower reduction temperatures. Additionally, the material demonstrated long-term stability after 24 h of reaction. This work corroborated that a low-surface-area material such as SiC was a suitable support for the nanosized Ru catalysts, allowing operation at one of the lowest reaction temperatures for hydrogen production from ammonia decomposition in this field [55].

4.1.2. Rare-Earth Oxide Supports

On the other hand, other supports based on rare-earth oxides, especially ceria (CeO_2) and lanthanum oxide (La_2O_3), have been also employed as supports for Ru catalysts [14,56–60]. These metal oxides are conventional supports characterized by a low cost, high basicity and great capacity to produce strong metal–support interactions that protect against metal sintering, due to the oxygen vacancies of the materials. However, these metal oxides do not show high surface area values (around $10\text{--}20\text{ m}^2\text{ g}^{-1}$).

Hu et al. [56] discovered that Ru (7 wt.%) supported on CeO_2 (nanorods) showed a catalytic activity over 8 times higher than that of the counterpart system of Ru supported on carbon nanotubes (CNTs), the most active catalysts in the state-of-the-art literature when feeding pure ammonia. The strong metal–support interactions as well as the generation of small particles ($\sim 3\text{ nm}$) on the Ru/ CeO_2 caused an improvement in the ammonia conversion. Additionally, the utilization of sodium (Na) as a promoter reduced the metal size and enhanced the electronic state of Ru, increasing the ammonia conversion at low temperatures. Meanwhile, Furusawa et al. [57] prepared a chlorine-free Ru/ CeO_2 catalyst (5 wt.%) by incipient wetness impregnation and subsequent washing with 0.01 M of aqueous ammonia. Moreover, the influence of the promoter/Ru molar ratio was adjusted together with the reduction conditions (with or without H_2 pretreatment). The addition of a promoter, cesium (Cs), improved the catalytic activity because of a reduction in the metal particle size ($\sim 2\text{ nm}$), with or without H_2 pretreatment, and an increase in the amount of strong basic sites. Therefore, the catalyst with Cs/Ru = 0.43 molar ratio, treated in Ar at $500\text{ }^\circ\text{C}$, resulted in 80% ammonia conversion at $300\text{ }^\circ\text{C}$ at $2000\text{ mL-NH}_3\text{ g}_{\text{cat}}^{-1}\text{ h}^{-1}$. In both studies, promoters provided easy desorption of N-adatoms from the surface, which was considered the rate-determining step.

Regarding the use of La_2O_3 as support for Ru catalysts, Huang et al. [58] reported that the synthesis method of La_2O_3 influenced the production of hydrogen from ammonia. They observed that the Ru/ La_2O_3 -700-i (4.8 wt.%) catalyst, prepared by the impregnation method, exhibited a 90.7% ammonia conversion for 84 h at $525\text{ }^\circ\text{C}$ and $18,000\text{ mL-NH}_3\text{ g}_{\text{cat}}^{-1}\text{ h}^{-1}$, whereas an ammonia conversion of 77% was achieved with Ru/ La_2O_3 -700-p (4.8 wt.%) catalyst prepared by a one-step pyrolysis method. The superior activity of the material synthesized by the impregnation method was related to the presence of a high-purity La_2O_3 phase, as revealed by X-ray diffraction (XRD) characterization, and the slight variation in the surface area, $20.9\text{ m}^2\text{ g}^{-1}$ (Ru/ La_2O_3 -700-i) versus $8.0\text{ m}^2\text{ g}^{-1}$ (Ru/ La_2O_3 -700-p). The addition of potassium hydroxide (KOH) improved the performance of the catalyst.

Considering the utilization of rare-earth oxides as catalytic supports, it is well known that rare-earth oxides present a small surface area ($10\text{--}30\text{ m}^2\text{ g}^{-1}$), although they are usually employed as catalytic supports for ammonia decomposition [43,44,59,61]. In fact, Im et al. [59] compared the performance of different metal oxide supports and their dependence on the basic properties of Ru catalysts ($\sim 2\text{ wt.}\%$). The ammonia conversion at $500\text{ }^\circ\text{C}$ and $6000\text{ mL-NH}_3\text{ g}_{\text{cat}}^{-1}\text{ h}^{-1}$ decreased in order of Ru/ $\text{La}_2\text{O}_3 > \text{Ru/Pr}_x\text{O}_y > \text{Ru/Sm}_2\text{O}_3 \sim \text{Ru/Gd}_2\text{O}_3 > \text{Ru/Y}_2\text{O}_3 > \text{Ru/Yb}_2\text{O}_3$ catalysts. It was related to the decrease (in the same order) in the total basic sites and the basic strength of the catalysts. The basic properties influenced the electron state of Ru, enhancing the electron donation from the support to the active phase and thus enhancing the activity. This was corroborated by NH_3 temperature-programmed surface reaction (NH_3 -TPSR) and the promotion of the desorption step of N atoms. Meanwhile, Zhang et al. [62] developed a solid milling method, which consisted of milling ruthenium oxide (RuO_2) and samarium (III) hydroxide ($\text{Sm}(\text{OH})_3$) in a mortar by hand for 10 min, to obtain Ru- Sm_2O_3 -m (4 wt.%) with a surface area of $28.5\text{ m}^2\text{ g}^{-1}$. However, it was found that other synthesis methods exhibited a much higher activity due to the greater interaction between Ru and samarium oxide (Sm_2O_3) support.

On the other hand, Le et al. [63] recently used the deposition–precipitation method to develop a novel $\text{La}_x\text{Ce}_{1-x}\text{O}_y$ composite as support for 1.8 wt.% of Ru loading. The optimal catalyst presented a 0.33 and 0.67 molar ratio of La and Ce with a surface area of

$31 \text{ m}^2 \text{ g}^{-1}$, similar to the rest of the catalysts. However, this material showed a small Ru size with a strong metal–support interaction and optimized acidity–basicity properties, which enhanced the rate-determining step. This was corroborated by density functional theory (DFT) calculations. Hence, this catalyst achieved 80% ammonia conversion at $500 \text{ }^\circ\text{C}$ and $54,000 \text{ mL-NH}_3 \text{ g}_{\text{cat}}^{-1} \text{ h}^{-1}$.

4.1.3. ABO_3 Perovskites as Ru Supports

In light of the utilization of composites as catalytic supports, a series of ABO_3 perovskite materials, $\text{Sr}_{1-x}\text{Y}_x\text{Ti}_{1-y}\text{Ru}_y\text{O}_{3-\delta}$ ($x = 0, 0.08$ and 0.16 ; $y = 0, 0.04, 0.07, 0.12, 0.17$ and 0.26) were synthesized by a modified Pechini method and tested for ammonia dehydrogenation; their surface area varied from 25 to $40 \text{ m}^2 \text{ g}^{-1}$ [64]. The influence of A or B site substitution on the catalytic ammonia dehydrogenation activity was determined by varying the quantity of either A or B site cations. The authors suggested that the simultaneous formation of SrRuO_3 and Ru^0 generated suitable interactions, although they did not give any information about this. However, ammonia decomposition was improved and the $\text{Sr}_{0.84}\text{Y}_{0.16}\text{Ti}_{0.92}\text{Ru}_{0.08}\text{O}_{3-\delta}$ (8 mol % of Ru) displayed a conversion of 96% at $500 \text{ }^\circ\text{C}$ and $10,000 \text{ mL-NH}_3 \text{ g}_{\text{cat}}^{-1} \text{ h}^{-1}$ for long reaction times. More recently, a $\text{La}_{1-x}\text{Sr}_x\text{AlO}_3$ typical perovskite-oxide, prepared by citrate sol–gel method, was reported to be an efficient support, with small surface area ($\sim 18 \text{ m}^2 \text{ g}^{-1}$), for Ru (3 wt.%) catalysts [65]. The properties of the supports were modulated and adjusted by tailoring the cation substitution of La^{3+} by Sr^{3+} , and it was discovered that the activity strongly depended on the nature of $\text{La}_{1-x}\text{Sr}_x\text{AlO}_3$. In particular, characterization results of $\text{Ru}/\text{La}_{0.8}\text{Sr}_{0.2}\text{AlO}_3$ showed the highest electro-rich state of metallic Ru, which promoted the reaction mechanism.

Additionally, Zhiqiang et al. [66] have employed different alkali metal silicates A_2SiO_3 ($\text{A} = \text{Li}, \text{Na}$ and K) as supports prepared by a sol–gel method. The formation of a silicate structure resulted in a reduction in the surface area ($< 10 \text{ m}^2 \text{ g}^{-1}$). The K_2SiO_3 material, with the lowest surface area ($3.2 \text{ m}^2 \text{ g}^{-1}$), exhibited the highest catalytic activity (60.5% NH_3 conversion at $450 \text{ }^\circ\text{C}$ and $30,000 \text{ mL-NH}_3 \text{ g}_{\text{cat}}^{-1} \text{ h}^{-1}$). The maximum performance was caused by an increase in the strength and number of basic sites and suitable metal–support interactions, which were related to the highest content of oxygen vacancies. In addition, these properties led to small Ru particle size.

4.1.4. Metal Oxide Supports

Based on layered double hydroxides (LDHs), Zhao et al. [67] recently employed calcium (Ca)–alumina (Al) LDHs with low surface area for ammonia decomposition. The LDHs allowed the synthesis of nanoparticles with designed morphological and structural characteristics despite their relatively inert oxides. The influence of the synthesis method on ammonia decomposition was studied. Firstly, an aqueous solution of Ru was employed ($\text{Ru}/\text{CaAlO}_x\text{-w}$), and secondly, an ethanol solution of Ru was incorporated by impregnation ($\text{Ru}/\text{CaAlO}_x\text{-e}$). Thus, spherical or elliptical Ru particles were embedded with the CaAlO_x with strong metal–support interactions when water was utilized, while spots of large diameter were obtained with ethanol. In this sense, the spherical or elliptical Ru particles and the higher metal–support interaction enhanced the reaction at low temperatures.

Another very interesting metal oxide with a low surface area ($\sim 30 \text{ m}^2 \text{ g}^{-1}$) employed as support for Ru is zirconia (ZrO_2). This material is an amphoteric support because it acts as a base or an acid, i.e., it is capable of donating and accepting protons, and hence, it could not be considered an ideal support for hydrogen generation from ammonia decomposition [34]. However, the characteristics of this material can be easily altered by chemical or physical routes [68].

In this sense, different barium-doped zirconia (Ba-ZrO_2) supports were compared as support for 3 wt.% of Ru catalysts [68]. It was found that the material synthesized by sol–gel process ($\text{Ru}/\text{Ba-ZrO}_2$) in comparison with the support prepared by conventional immersion ($\text{Ru-Ba}/\text{ZrO}_2$) demonstrated a higher activity in the NH_3 decomposition reaction. The superior ammonia conversion of $\text{Ru}/\text{Ba-ZrO}_2$ (100% at $450 \text{ }^\circ\text{C}$ and $3000 \text{ mL-NH}_3 \text{ g}_{\text{cat}}^{-1} \text{ h}^{-1}$) versus

that of Ru-Ba/ZrO₂ (10% at the same conditions) was a consequence of the formation of BaZrO₃ phase, which improved the electron transfer from the support to Ru, hence accelerating the rate-determining step of the reaction.

In another work, Hu et al. [69] reported a novel metal–organic framework (MOF) prepared from a zirconia precursor, leading to a mesoporous crystalline zirconia (MPC-ZrO₂) of low area (2 m² g^{−1}). They studied the influence of Ru loading (0.8–6.5 wt.%) as well as the Cs loading (2.5–10 wt.%). The synthesis of Ru catalysts by incipient wetness impregnation method allowed obtaining small Ru nanoparticles (~3 nm) confined within the rigid crystalline MPC-ZrO₂ with strong metal–support interactions. As expected, the NH₃ conversion increased with the Ru loading until a maximum value was obtained for 5 wt.% of Ru, as shown in Table 1. Moreover, 5 wt.% of Cs was selected as the optimal Cs loading because a further increase decreased the activity, which may be due to the blockage of the active sites. On the other hand, the basic properties of zirconia were controlled by doping with La and alkaline-earth metals, using a co-precipitation method while Ru (0.5 wt.%) was incorporated by wet impregnation [70]. The addition of La and strontium (Sr) increased weak, medium and strong basic sites, whereas magnesium (Mg) and Ca only improved weak and medium basic sites.

On the other hand, the most used support in this reaction is alumina oxide (Al₂O₃); nonetheless, it generally shows a large surface area [14,34]. To the best of our knowledge, only one recent manuscript described a Ru catalyst supported on Al₂O₃ doped with La (10Ru-La(50)- Al₂O₃) with a low surface area (23.3 m² g^{−1}) [71]. The authors suggested that a new phase, LaAlO₃, formed during the synthesis method strongly interacted with Ru active sites, facilitating ammonia dehydrogenation even at low temperatures. This material achieved an ammonia conversion of 68.9% at 400 °C and 2300 mL-NH₃ g_{cat}^{−1} h^{−1}.

Taking into account the utilization of alkaline-earth metal oxides with low surface area as supported Ru catalysts, magnesia (MgO) and calcium oxide (CaO) were reported [54]. The work carried out by Sayas et al. [54] optimized Ru/CaO catalysts promoted with potassium (5–15 wt.%) to perform the ammonia decomposition reaction at high pressure. Commercial CaO and MgO presented a small surface area (values between 4–30 m² g^{−1}), and Ru (1–7 wt.%) was incorporated by incipient wetness impregnation. In spite of the specific area, CaO showed a large number of basic sites and stronger basic sites, and it allowed the generation of an average Ru nanoparticle size of 6 nm. The reaction was also performed at atmospheric pressure, and the catalysts were optimized. The maximum activity (61.0% conversion at 400 °C and 9000 mL-NH₃ g_{cat}^{−1} h^{−1}) was achieved with 3 wt.% and 10 wt.% of Ru and K loadings, respectively, which was a consequence of the suitable Ru nanoparticle size.

4.2. Non-Noble-Metal-Based Catalysts

In order to avoid the utilization of ruthenium as the active phase because of its high price and environmental impact, as mentioned in Section 2, other non-noble metals (e.g., Ni, Co, Fe, Cu, molybdenum (Mo)) should be considered for the design of heterogeneous catalysts for the ammonia decomposition reaction. Note also that although these materials did not exhibit an activity as high as that of Ru, they are economically viable and eco-friendly [14,34,55].

Table 1. Catalytic activity of ruthenium-based catalysts for H₂ production from NH₃ decomposition performance at 1 atm.

Catalyst	Ru Loading (wt.%)	S _{BET} (m ² g ⁻¹)	GHSV (mL·g _{cat} ⁻¹ ·h ⁻¹)	NH ₃ Inlet Flow (%)	T (°C)	NH ₃ Conversion (%)	H ₂ Formation Rate (mmol H ₂ g _{cat} ⁻¹ min ⁻¹)	Ref.
2.5Ru/SiC-600-N ₂ flow	2.5	25.9	60,000	5	350	80.2	2.53	[40]
2.5Ru/SiC-600-air flow	2.5	26.9	60,000	5	350	72.3	2.37	
2.5Ru/SiC-600-static air	2.5	25.6	60,000	5	350	67.5	2.06	
2.5Ru/SiC-600-non-calcined	2.5	29.3	60,000	5	350	69.8	2.17	
1Ru/SiC-400-N ₂ flow	1.0	28.8	60,000	5	350	59.6	2.00	
2.5Ru/SiC-400-N ₂ flow	2.5	26.3	60,000	5	350	98.7	3.30	
5Ru/SiC-400-N ₂ flow	5.0	25.5	60,000	5	350	86.6	2.90	
1Ru/SiC-600-N ₂ flow	1.0	28.8	60,000	5	350	41.5	1.31	
5Ru/SiC-600-N ₂ flow	5.0	25.5	60,000	5	350	89.9	2.91	
Ru/CeO ₂ -NR	7.0	15.0	6000	29	350	23.0	1.54	
Ru-Na/CeO ₂ -NR	7.0	10.0	6000	29	350	25.0	1.67	
Ru/CeO ₂	5.0	14.6	2000	100	350	60.0	26.80	[57]
Ru-Cs/CeO ₂	5.0	13.1	2000	100	350	98.0	44.00	
Ru/La ₂ O ₃ -700-i	4.8	20.9	18,000	100	400	40.0	8.04	[58]
Ru/La ₂ O ₃ -700-p	4.8	8.0	18,000	100	400	35.0	5.02	
Ru/La ₂ O ₃ -700-i-K	4.8	-	18,000	100	400	50.0	10.04	
Ru/Y ₂ O ₃	2.0	29.2	6000	100	500	82.6	5.53	[59]
Ru/La ₂ O ₃	2.1	22.2	6000	100	500	95.6	6.40	
Ru/Pr _x O _y	2.0	15.3	6000	100	500	93.0	6.23	
Ru/Sm ₂ O ₃	2.1	9.4	6000	100	500	85.6	5.73	
Ru/Gd ₂ O ₃	2.0	11.6	6000	100	500	85.2	5.71	
Ru/Yb ₂ O ₃	1.9	25.6	6000	100	500	28.6	1.92	
4Ru/Sm ₂ O ₃ -m	3.5	28.5	30,000	100	450	15.7	4.90	[62]
Ru/La _{0.33} Ce _{0.67}	1.8	31.0	6000	100	400	93.0	6.23	[63]
Ru/La _{0.5} Ce _{0.5}	1.8	28.0	6000	100	400	86.0	5.76	
Ru/La	1.8	30.0	6000	100	400	41.0	2.75	
Sr _{0.92} Y _{0.08} Ti _{0.88} Ru _{0.12} O _{3-δ}	6.1 mol %	33.5	10,000	100	350	2.3	0.25	[64]
Sr _{0.92} Y _{0.08} Ti _{0.74} Ru _{0.26} O _{3-δ}	12.4 mol %	24.5	10,000	100	350	18.4	2.05	
Sr ₁ Y ₀ Ti _{0.91} Ru _{0.09} O _{3-δ}	4.22 mol %	31.1	10,000	100	350	3.2	0.36	

Table 1. Cont.

Catalyst	Ru Loading (wt.%)	S _{BET} (m ² g ⁻¹)	GHSV (mL·g _{cat} ⁻¹ ·h ⁻¹)	NH ₃ Inlet Flow (%)	T (°C)	NH ₃ Conversion (%)	H ₂ Formation Rate (mmol H ₂ g _{cat} ⁻¹ min ⁻¹)	Ref.
Ru/LaAlO ₃	3	18.1	30,000	100	500	50.0	75.00	[65]
Ru/La _{0.9} Sr _{0.1} AlO ₃	3	18.4	30,000	100	500	60.0	90.00	
Ru/La _{0.8} Sr _{0.2} AlO ₃	3	18.8	30,000	100	500	71.6	107.40	
Ru/La _{0.7} Sr _{0.3} AlO ₃	3	18.5	30,000	100	500	55.7	83.55	
Ru/Li ₂ SiO ₃	3.4	8.5	30,000	100	450	30.0	10.4	[66]
Ru/Na ₂ SiO ₃	3.5	9.6	30,000	100	450	52.0	17.8	
Ru/K ₂ SiO ₃	3.2	3.6	30,000	100	450	60.5	20.3	
Ru/CaAlOx-e	3.5	11.3	6000	100	400	8.5	0.57	[67]
Ru/CaAlOx-w	3.5	11.8	6000	100	400	38.0	2.54	
Ru/ZrO ₂	3.0	38.6	3000	100	500	20.0	1.34	[68]
Ru/Ba-ZrO ₂	3.0	25.4	3000	100	500	100.0	3.35	
Ru-Ba/ZrO ₂	3.0	6.3	3000	100	500	10.0	0.67	
0.8Ru/MPC-ZrO ₂	0.8	8.0	6000	29	350	0.0	0.00	[69]
2Ru/MPC-ZrO ₂	2.0	20.0	6000	29	350	1.1	0.07	
3.5Ru/MPC-ZrO ₂	3.5	18.0	6000	29	350	3.9	0.26	
5Ru/MPC-ZrO ₂	5.0	12.0	6000	29	350	6.5	1.59	
6.5Ru/MPC-ZrO ₂	6.5	10.0	6000	29	350	2.1	0.14	
5Ru2.5Cs/MPC-ZrO ₂	5.0	11.0	6000	29	350	4.1	0.27	
5Ru5Cs/MPC-ZrO ₂	5.0	7.5	6000	29	350	19.4	4.47	[69]
5Ru10Cs/MPC-ZrO ₂	5.0	3.0	6000	29	350	5.8	0.39	
Ru/ZrO ₂	0.5	28.0	4600	100	400	60.4	5.13	[70]
Ru/ZrO ₂	2.0	4.9	6000	100	500	0	0	[59]
Ru/La(50)-Al ₂ O ₃ or LaAlO ₃	0.7	23.3	2300	10	400	68.5	1.76	[71]
5Ru10K/MgO	4.8	32.0	9000	100	400	39.4	3.96	[54]
1Ru10K/CaO	0.9	6.0	9000	100	400	8.5	0.85	
2Ru10K/CaO	1.8	7.0	9000	100	400	40.0	4.02	
3Ru10K/CaO	2.8	5.0	9000	100	400	61.0	6.13	
5Ru10K/CaO	4.7	4.0	9000	100	400	53.7	5.39	
7Ru10K/CaO	6.6	8.0	9000	100	400	35.0	3.52	
3Ru/CaO	2.9	10.0	9000	100	400	5.0	0.50	
3Ru5K/CaO	2.8	5.0	9000	100	400	20.0	2.01	
3Ru15K/CaO	2.7	5.0	9000	100	400	60.0	6.03	

4.2.1. Novel Silicon Carbide Support

Based on the excellent properties delivered by novel SiC as support for Ru catalysts, Pinzon et al. [42] also synthesized, for the first time, Co (5 wt.%) supported on SiC. Additionally, different promoters (alkaline, alkaline-earth and rare-earth metals) have been studied and optimized. The addition of certain promoters could reduce the reaction temperature in Co/SiC catalysts. It was found that the addition of 1 wt.% of K and La improved the ammonia conversion, whereas the addition of other promoters did not enhance (Cs and Ce) or even decreased (Mg and Ca) the activity with respect to the unpromoted catalyst. For instance, Cs did not increase the basic sites, and Ce could be inhibited by hydrogen. Regarding Mg and Ca, the metal dispersion was lower. The basicity and electron-donor properties of Co catalysts were improved by an optimized K amount of 1 wt.%, which enhanced the activity with respect to La. Nonetheless, an increase in the K loading led to the blockage of the active sites. Thus, Co-1K/SiC was found to be an excellent and stable catalyst providing a conversion close to 100% at 450 °C and 60,000 mL-NH₃-Ar g_{cat}⁻¹ h⁻¹ for one day of reaction.

4.2.2. Rare-Earth Oxide Supports

Other less novel supports with low surface area are based on metal oxides, mainly rare-earth oxides (La₂O₃, CeO₂, Y₂O₃, Sm₂O₃ and Gd₂O₃). These have been widely employed as supports for cobalt and nickel catalysts [72–76]. In fact, for the first time, Okura et al. [74] prepared a screening of Ni (10 wt.%) catalysts supported on rare-earth oxides by the conventional impregnation method for the ammonia decomposition reaction. These materials showed a small surface area (<10 m² g⁻¹) with an adequate activity in this reaction as a consequence of the low effect of hydrogen inhibition. In particular, Ni/Y₂O₃ exhibited the best catalytic activity owing to the lowest amount of strongly adsorbed hydrogen. In another work, the influence of alkaline-earth metals (Mg, Ca, Sr and Ba) over Ni/Y₂O₃ catalyst on the reaction was also studied by the same group [72]. It was found that Sr and Ba enhanced the activity of Ni catalysts since alkaline-earth metals interacted strongly with Ni. This interaction improved the basic properties favoring the desorption of nitrogen atoms (rate-determining step) and accelerating the reaction mechanism at low temperatures.

Other authors investigated the influence of synthesis conditions on Ni [73] and Co [75] supported on La₂O₃ as well as the influence of the MgO as a promoter. First, the calcination temperature of lanthanum oxide affected the catalytic activity of Ni as follows: 10Ni/La₂O₃-450 > 10Ni/La₂O₃-550 > 10Ni/La₂O₃-650 ~ 10Ni/La₂O₃-750 ~ 10Ni/La₂O₃-850, which was associated with the relatively higher specific surface area and the higher numbers of basic sites and oxygen species in the surface [73]. In this work, the incorporation of Mg, added by surfactant-templated method, increased the basicity of the catalysts, which improved the Ni electron density, enhancing the reaction and yielding a conversion of 82% at 550 °C with a nickel loading of 40 wt.%. Podila et al. [75] investigated the effect of the calcination atmosphere in Co (5 wt.%) supported on MgO-La₂O₃ prepared by coprecipitation from metal nitrate solutions under high supersaturation. The material calcined in a N₂ atmosphere (5CMLa-N₂) had higher surface metal concentration and the strongest metal-support interaction, achieving a good catalytic performance. On the other hand, the morphology of ceria also influenced the activity of cobalt catalysts and the surface area, which ranged between 20 and 50 m² g⁻¹ depending on the form of the crystallites [76]. Hence, CeO₂ nanocubes showed the lowest area (20 m² g⁻¹) but had the best redox properties, thereby exhibiting a suitable activity (67% ammonia conversion at 550 °C).

4.2.3. ABO₃ Perovskites as Supports and Catalytic Precursors

It is well known that rare-earth oxides promote the catalytic effect of nickel and cobalt [14,34,49,74,77]. Nonetheless, they exhibit a very small surface area, hindering the production of small Ni/Co sizes, which in turn decreases the activity. Therefore, the benefits of perovskites as catalyst precursors and/or supports were investigated to develop materials with better characteristics than the main metal oxides.

The utilization of perovskite-type oxides (LaBO_3) as catalytic precursors of Ni catalysts for ammonia decomposition was firstly carried out by Muroyama et al. [78]. These perovskite-type oxides seem to be highly promising precursors in this reaction because the final catalysts (perovskite-derived catalysts) were obtained after the reduction of perovskites under hydrogen flow [43]. That work provided new insight into the design of diverse, economic and efficient catalysts to achieve a high activity at low temperature and enhanced the perspective of ammonia as a hydrogen carrier toward the “hydrogen economy”, despite the small surface area ($<30 \text{ m}^2 \text{ g}^{-1}$) of these perovskite-derived catalysts.

Recently, Pinzon et al. [43] found that in the self-combustion synthesis method, both the fuel–metal nitrates molar ratio and the calcination temperature played an important role in the properties of the resulting perovskites. In this sense, a citric acid–metal nitrate molar ratio equal to 1 allowed the generation of a LaNiO_3 perovskite without impurities and with suitable physicochemical properties (higher specific surface area, $\sim 11 \text{ m}^2 \text{ g}^{-1}$, and basicity, $17.8 \mu\text{mol CO}_2 \text{ g}^{-1}$, without impurities, La_2NiO_4). Moreover, the calcination temperature affected the size of the final nickel/cobalt catalysts. A calcination temperature of $650 \text{ }^\circ\text{C}$ led to small and well-dispersed Ni^0 . For Co perovskites, calcination temperature below $900 \text{ }^\circ\text{C}$ did not influence on the size of Co^0 after reduction. Therefore, Ni and Co perovskite-derived catalysts yielded an excellent ammonia conversion, 98.9% and 97%, respectively, at $450 \text{ }^\circ\text{C}$ and $75,000 \text{ mL-NH}_3\text{-Ar g}_{\text{cat}}^{-1} \text{ h}^{-1}$ with a suitable stability for one day.

Aiming to improve the activity of Ni catalysts derived from perovskite, the addition of different dopant agents could increase the basicity, among other properties. Thus, the partial substitution of La cation by Ce [44,79] or by Mg [44] was studied. For that, $\text{La}_x\text{A}_{1-x}\text{NiO}_3$, where A = Ce or Mg and $x = 0, 0.1, 0.9$ and 1 (molar basis), was synthesized and examined in the production of hydrogen from ammonia. It was observed that the addition of the Ce and Mg improved the basicity and the further decrease in the metal size after reduction, which enhanced the catalytic performance. Mainly, a dopant amount of 0.9 molar basis of Ce and Mg led to catalysts with a nickel size of 4.6 nm and 4.1 nm, respectively, whereas $21.2 \mu\text{mol CO}_2 \text{ g}^{-1}$ and $64.6 \mu\text{mol CO}_2 \text{ g}^{-1}$, respectively, of total basic sites were obtained. These nickel catalysts yielded a conversion of 96% ($\text{La}_{0.1}\text{Ce}_{0.9}\text{NiO}_3$) and 98% ($\text{La}_{0.1}\text{Mg}_{0.9}\text{NiO}_3$) at low temperatures ($400 \text{ }^\circ\text{C}$) for 40 h of reaction, exhibiting a good stability without deactivation. Mg was selected as the best dopant of nickel perovskite, mainly due to the virtuous synergic effect between Ni, Mg and La, which showed a higher basicity and a higher capacity to desorb N_2 [44].

The application of perovskite-type oxides as supports for nickel and cobalt catalysts has been proposed by different authors [80,81]. In both studies, the influence of the variation of different alkaline, alkaline-earth and rare-earth metals of the ABO_3 formulation on the ammonia decomposition was investigated, and these materials displayed a small surface area ($<20 \text{ m}^2 \text{ g}^{-1}$) owing to the high calcination temperature ($1100 \text{ }^\circ\text{C}$) required for their synthesis [81].

On the one hand, XCeO_3 (X = Mg, Ca, Sr, Ba) perovskite-type oxides were synthesized by the combustion method while cobalt (5 wt.%) was incorporated by wet impregnation [80]. It was found that the activity increased as the electronegativity of the X elements decreased, and the BaCeO_3 support was the one that presented the highest catalytic activity because of the highest conductivity, moderate metal–support interaction and moderate basicity.

On the other hand, Okura et al. [81] prepared several formulations of perovskites using the solid-state reaction or the citric acid complex methods. ANbO_3 (A = Na and K) and AETiO_3 (AE = Ca, Sr and Ba) were prepared by the first method, while REAlO_3 (RE = La, Sm and Gd), AEMnO_3 and AEZrO_3 were prepared by the latter. The nickel (40 wt.%) was incorporated by wet impregnation. The supports containing Nb and Mn exhibited a lower conversion at $550 \text{ }^\circ\text{C}$, whereas REAlO_3 , AETiO_3 and AEZrO_3 supports increased the activity, mainly due to the electronic state of nickel species. Additionally, the AEZrO_3 supports exhibited a higher amount of basic sites owing to the smaller electronegativity of Zr. Regarding the electronegativity of the AE elements, Ba and Sr (lower electronegativity in comparison with Ca) increased the number of basic sites and hence

were responsible for the higher catalytic activity of Ni/BaZrO₃ and Ni/SrZrO₃. They displayed conversions of 93% (Ni/SrZrO₃) and 95% (Ni/BaZrO₃) at 550 °C.

4.2.4. Metal Oxide Supports

Other precursors, based on hydrotalcite materials (derived from layered double hydroxides), allowed the synthesis of catalysts with controlled accessibility to the structure, after high-temperature reduction [82]. Nickel hydrotalcites based on Ca²⁺ and Al³⁺ cations (Ni_xCa₂Al₁-LDHs-ST, x = 0.1, 0.3, 0.5, 1 and 2) were prepared by mixing the corresponding nitrates with a Ca²⁺/Al³⁺ atomic ratio equal to 2, using a precipitating agent (2 M of NaOH, pH = 12). Then, the precipitant was transferred into a Teflon vessel (100 °C for 36 h) and the product was centrifugated, washed and dried overnight. It was found that the gradual incorporation of Ni altered the structure of the Ca₂Al₁-LDHs to hydrobomkulite and finally to takovite. This transformation led to an increase in the amount of B5-type sites, which improved the NH₃ decomposition (55% ammonia conversion at 550 °C and 10,000 mL-NH₃ g_{cat}⁻¹ h⁻¹). Despite the low area of the catalysts (30.1 m² g⁻¹), hydrotalcites seem to be a good precursor for the design of heterogeneous catalysts presenting better catalytic properties than those obtained by the conventional impregnation method (Ni₁/Ca₂Al₁-LDHs-IM).

In light of the structure of the supports, fluorite-type oxides with a face-centered cubic crystal structure (for example, ceria–zirconia alloys, CZY) showed good redox properties, high thermal stability and good capacity to disperse the metals, despite the small area (values < 30 m² g⁻¹) [83]. Ni, Co and Ni-Co (10 wt.%) catalysts were prepared by incipient wetness impregnation over CZY and tested on ammonia decomposition. Noticeably, the bimetallic catalysts with 9 wt.% of Co and 1 wt.% of Ni (Ni₁Co₉/CZY) resulted in the highest activity at 60,000 mL-NH₃ g_{cat}⁻¹ h⁻¹ with almost 100% conversion at 600 °C for 72 h, owing to the formation of a Ni-Co alloy with suitable metal dispersion (20.3%). The authors claimed that the synthesis of these metal oxides (CZY) was an eco-friendly and affordable process.

Based on an economic, abundant and low-surface-area material, fresh mica nanosheets (K_{0.75}Al₂Si₄O₁₀(OH)₂) have been employed as support for nickel catalysts (20–30 wt.% prepared by wet impregnation) in the reaction [84]. The catalytic activity was improved by the two-dimensional structure of mica since the mass transfer was favored. Another natural nanostructural material, attapulgite (ATP), has been used as support for Ni catalysts (50 wt.% prepared by homogeneous precipitation method) [85]. This synthesis developed materials with a low surface area (<10 m² g⁻¹) that showed good performance in the ammonia decomposition, exhibiting a conversion of 65% at 600 °C. The strong metal–support interaction was responsible for the adequate activity.

Im et al. [50] prepared different aluminate-based compounds (AM-Al-O, AM = Mg, Ca, Sr and Ba) modified with alkaline-earth metals by solid-state reaction. These were investigated as supports for nickel (20 wt.%) catalysts. Similarly to what was mentioned above, the basic properties of the materials changed with the different metals; the Ni/Sr-Al-O and Ni/Ba-Al-O catalysts were the most basic materials, providing a higher performance in the production of hydrogen from ammonia.

4.2.5. Metal Imide Supports

Recently, the utilization of metal imides (Mg₃N₂, CaNH and BaNH) as support for Co catalysts in the ammonia decomposition reaction has received attention. The catalysts were prepared following the procedure described in [86], showing a low surface area. The Co-CaNH material showed the highest specific surface area among the three materials but a lower activity than that of Co-BaNH. The highest activity of Co-BaNH was related to an intermediate phase (Co-N-Ba) which enhanced the energy-efficient reaction pathway.

4.2.6. Other Low-Surface-Area Supports

On the other hand, pure oxides such as Co_3O_4 (100Co) [87] and NiO [88,89] have been studied as catalysts in spite of their low area ($<30 \text{ m}^2 \text{ g}^{-1}$). However, the catalytic activity was low ($<20\%$ ammonia conversion at $550 \text{ }^\circ\text{C}$) at lower temperatures, as can be observed in Table 2, caused by the morphological defects of these materials and their poor stability.

Other monometallic catalysts with small surface areas were based on Fe and Mo supported on commercial carbon nanofibers (CFs). The materials were prepared by the impregnation method of different metal loadings (4–14 wt.%) providing an area below $40 \text{ m}^2 \text{ g}^{-1}$ [90]. Mo catalysts displayed lower conversion than Fe catalysts over a conventional heated reaction system. However, the activities of both catalysts improved at lower temperatures in the microwave reaction system because of the formation of carbide species (Fe_2C and Mo_2C), which are found to enhance the transfer of energy to the active phase.

4.3. Bimetallic Catalysts and Metal Catalysts

Finally, the utilization of non-noble bimetallic catalysts with low surface area has been also investigated (Table 2). It has been established that the apparent activation energy (E_a) of the bimetallic catalysts was lower than that of the monometallic catalysts, enhancing the ammonia conversion [14].

In this sense, mono- and bimetallic perovskites ($\text{LaCo}_{1-x}\text{Ni}_x\text{O}_3$, $x = 0, 0.2, 0.4, 0.6, 0.8$ and 1 molar basis) were synthesized and tested as catalyst precursors for ammonia decomposition [44]. However, bimetallic perovskites originated a higher particle size of Co^0/Ni^0 (in the range of 7.8–5.7 nm) than the pure LaNiO_3 (4.2 nm), which did not improve the activity. Both impurities and a lower amount of active sites were detected on bimetallic perovskites, which also decreased the ammonia conversion. The higher catalytic activity of nickel perovskite-derived catalysts versus cobalt perovskite-derived catalysts has been corroborated by Podila et al. [79].

As illustrated in Section 3, the alloy between Co and Mo is near the volcano curve, with a suitable N binding energy to easily desorb nitrogen species, the active phase being $\text{Co}_3\text{Mo}_3\text{N}$ [17,91]. Duan et al. [91] studied the effect of the calcination atmosphere on metal amine metallate ($\text{Co}(\text{en})_3\text{MoO}_4$) precursors to obtain an active catalyst based on Co-Mo. They selected argon (Ar) and air (Air) as the calcination atmosphere, which curiously affected the physicochemical properties. Indeed, the textural properties as well as the crystal phase were modified. The CoMo-Ar calcined catalyst showed magnetic properties and a higher surface area ($38.5 \text{ m}^2 \text{ g}^{-1}$) than CoMo-Air ($5.7 \text{ m}^2 \text{ g}^{-1}$). However, in the reduction step, the surface area changed, with CoMo-Ar and CoMo-Air showing $21 \text{ m}^2 \text{ g}^{-1}$ and $23.7 \text{ m}^2 \text{ g}^{-1}$, respectively, due to the transformation of the crystal phase. This change in surface area also took place during the reaction, since used CoMo-Ar-R displayed Co^0 and MoN, whereas used CoMo-Air-R showed MoO_2 , $\text{Co}_3\text{Mo}_3\text{N}$ and Co-Mo oxynitride. The presence of $\text{Co}_3\text{Mo}_3\text{N}$ led to a higher activity (74.3% of ammonia at $650 \text{ }^\circ\text{C}$ and $36,000 \text{ mL-NH}_3 \text{ g}_{\text{cat}}^{-1} \text{ h}^{-1}$) and stability. These authors affirmed that the prenitridation treatments (higher temperature prenitridation) allowed the generation of $\text{Co}_3\text{Mo}_3\text{N}$ as the active phase, without other metal oxides, and a higher surface area (although this area was not the key issue for increasing the activity).

In order to improve the activity of $\text{Co}_3\text{Mo}_3\text{N}$ materials, the influence of the addition of Cs to this material on ammonia decomposition was studied in detail [92]. The synthesis method involved the decomposition of hexamethylenetetramine (HMTA), Co, Ce and Mo salts under nitrogen at $700 \text{ }^\circ\text{C}$. It was corroborated that Cs dispersed highly over $\text{Co}_3\text{Mo}_3\text{N}$, improving its electronic state. This upgrading provided hydrogen and nitrogen desorption, and thus, the reaction mechanism was accelerated.

Table 2. Catalytic activity of non-noble catalysts for H₂ production from NH₃ decomposition performance at 1 atm.

Catalyst	Metal Loading (wt.%)	S _{BET} (m ² g ⁻¹)	GHSV (mL·g _{cat} ⁻¹ ·h ⁻¹)	NH ₃ Inlet Flow (%)	T (°C)	NH ₃ Conversion (%)	H ₂ Formation Rate (mmol H ₂ g _{cat} ⁻¹ min ⁻¹)	Ref.
5Co/SiC	5.0	24.0	60,000	5	350	27.20	0.90	
1Ca-5Co/SiC	5.0	29.0	60,000	5	350	22.80	0.76	
1Mg-5Co/SiC	5.0	30.0	60,000	5	350	29.60	0.99	
1La-5Co/SiC	5.0	24.0	60,000	5	350	27.40	0.92	
1K-5Co/SiC	5.0	19.0	60,000	5	350	33.10	1.12	[42]
1Cs-5Co/SiC	5.0	17.0	60,000	5	350	25.10	0.84	
1Ce-5Co/SiC	5.0	24.0	60,000	5	350	20.30	0.68	
0.5K-5Co/SiC	5.0	16.0	60,000	5	350	31.90	1.07	
1.5K-5Co/SiC	5.0	15.0	60,000	5	350	28.50	0.95	
Ni-Ca/Y ₂ O ₃	40.0	32.0	6000	100	500	44.00	2.95	[72]
10Ni/La ₂ O ₃ -450	10.0	25.0	30,000	100	550	59.0	19.75	
10Ni/La ₂ O ₃ -550	10.0	23.0	30,000	100	550	79.0	26.45	
10Ni/La ₂ O ₃ -650	10.0	14.0	30,000	100	550	60.0	20.09	
10Ni/La ₂ O ₃ -750	10.0	11.0	30,000	100	550	60.0	20.09	[73]
10Ni/La ₂ O ₃ -850	10.0	10.0	30,000	100	550	50.0	16.74	
LaNiO ₃	-	1.0	30,000	100	550	60.0	20.09	
40Ni/5MgLa	40.0	11.0	30,000	100	550	82.0	27.46	
Ni/Y ₂ O ₃	10.0	7.0	6000	100	450	18.00	1.21	
Ni/La ₂ O ₃	10.0	5.0	6000	100	450	12.00	0.80	
Ni/CeO ₂	10.0	4.0	6000	100	450	5.00	0.33	[74]
Ni/Sm ₂ O ₃	10.0	9.0	6000	100	450	15.00	1.00	
Ni/Gd ₂ O ₃	10.0	4.0	6000	100	450	17.00	1.14	
5CMLa-N ₂	5.0	33.0	6000	100	450	30.0	2.01	[75]
Co/CeO ₂ -nanocubes	5.0	20.0	6000	100	550	67.0	4.49	[76]

Table 2. Cont.

Catalyst	Metal Loading (wt.%)	S _{BET} (m ² g ⁻¹)	GHSV (mL·g _{cat} ⁻¹ ·h ⁻¹)	NH ₃ Inlet Flow (%)	T (°C)	NH ₃ Conversion (%)	H ₂ Formation Rate (mmol H ₂ g _{cat} ⁻¹ min ⁻¹)	Ref.
1 LaNiO ₃ 650	-	11.7	75,000	5	350	55.90	2.34	
0.5 LaNiO ₃ 650	-	8.7	75,000	5	350	36.70	1.54	
0.75 LaNiO ₃ 650	-	9.0	75,000	5	350	48.30	2.02	
1.25 LaNiO ₃ 650	-	9.9	75,000	5	350	33.60	1.41	
1 LaNiO ₃ 700	-	9.7	75,000	5	350	51.40	2.15	
1 LaNiO ₃ 750	-	7.8	75,000	5	350	41.60	1.74	[43]
1 LaNiO ₃ 900	-	3.2	75,000	5	350	30.20	1.26	
1 LaCoO ₃ 650	-	10.3	75,000	5	350	44.70	1.87	
2 LaCoO ₃ 700	-	13.4	75,000	5	350	41.80	1.75	
3 LaCoO ₃ 750	-	13.2	75,000	5	350	38.20	1.60	
4 LaCoO ₃ 900	-	3.5	75,000	5	350	34.00	1.42	
LaNi ₈₀ Co ₂₀ O ₃	-	12.0	75,000	5	350	30.00	1.26	
LaNi ₆₀ Co ₄₀ O ₃	-	12.0	75,000	5	350	31.70	1.33	
LaNi ₄₀ Co ₆₀ O ₃	-	9.0	75,000	5	350	41.10	1.72	
LaNi ₂₀ Co ₈₀ O ₃	-	9.0	75,000	5	350	37.10	1.55	
La ₉₀ Ce ₁₀ NiO ₃	-	11.0	75,000	5	350	33.20	1.39	
La ₁₀ Ce ₉₀ NiO ₃	-	29.0	75,000	5	350	59.10	2.47	[44]
CeNiO ₃	-	15.0	75,000	5	350	46.80	1.96	
La ₉₀ Mg ₁₀ NiO ₃	-	14.0	75,000	5	350	37.70	1.58	
La ₁₀ Mg ₉₀ NiO ₃	-	25.0	75,000	5	350	72.30	3.03	
MgNiO ₃	-	22.0	75,000	5	350	43.00	1.80	
La-Co	-	16.0	6000	100	350	4.00	0.27	
La-Ni	-	20.0	6000	100	350	10.00	0.67	[79]
La-Ce-Co	-	22.0	6000	100	350	4.00	0.27	
5Co-MgCeO	5.0	16.2	6000	100	550	35.0	3.86	
5Co-CaCeO	5.0	11.0	6000	100	550	55.2	4.53	
5Co-SrCeO	5.0	12.5	6000	100	550	41.1	4.67	[80]
5Co-BaCeO	5.0	15.7	6000	100	500	45.3	5.40	

Table 2. Cont.

Catalyst	Metal Loading (wt.%)	S _{BET} (m ² g ⁻¹)	GHSV (mL·g _{cat} ⁻¹ ·h ⁻¹)	NH ₃ Inlet Flow (%)	T (°C)	NH ₃ Conversion (%)	H ₂ Formation Rate (mmol H ₂ g _{cat} ⁻¹ min ⁻¹)	Ref.
Ni/Nb ₂ O ₅	40.0	7.4	6000	100	550	34.0	2.34	
Ni/NaNbO ₃	40.0	4.1	6000	100	550	40.0	2.68	
Ni/KNbO ₃	40.0	8.4	6000	100	550	36.0	2.41	
Ni/LaAlO ₃	40.0	9.9	6000	100	550	65.0	4.35	
Ni/SmAlO ₃	40.0	8.1	6000	100	550	83.0	5.56	
Ni/GdAlO ₃	40.0	4.6	6000	100	550	83.0	5.56	
Ni/MnO ₂	40.0	2.4	6000	100	550	44.0	2.95	
Ni/CaMnO ₃	40.0	6.6	6000	100	550	55.0	3.68	
Ni/SrMnO ₃	40.0	7.9	6000	100	550	50.0	3.35	
Ni/BaMnO ₃	40.0	7.2	6000	100	550	47.0	3.15	[81]
Ni/TiO ₂	40.0	12	6000	100	550	33.0	2.21	
Ni/CaTiO ₂	40.0	6.5	6000	100	550	37.0	2.48	
Ni/SrTiO ₂	40.0	5.5	6000	100	550	80.0	5.36	
Ni/BaTiO ₂	40.0	4.9	6000	100	550	75.0	5.02	
Ni/ZrO ₂	40.0	15.0	6000	100	550	27.0	1.81	
Ni/CaZrO ₃	40.0	6.0	6000	100	550	50.0	3.35	
Ni/SrZrO ₃	40.0	6.1	6000	100	550	93.0	6.03	
Ni/BaZrO ₃	40.0	7.5	6000	100	550	95.0	6.36	
Ni/Mg-Al-O	20.0	4.7	6000	100	450	6.7	0.45	
Ni/Ca-Al-O	20.0	16.7	6000	100	450	11.5	0.77	
Ni/Sr-Al-O	20.0	24.4	6000	100	450	16.5	1.10	[50]
Ni/Ba-Al-O	20.0	15.0	6000	100	450	24.8	1.66	
Ni/Ca ₂ Al ₁ -LDHs-ST	23.6	30.1	10,000	100	550	55.0	3.68	
Ni/Ca ₂ Al ₁ -LDHs-IM	23.6	13.5	10,000	100	550	25.0	1.67	[82]
Co/CZY	10.0	30.0	6000	100	350	6.5	0.44	
Ni/CZY	10.0	28.0	6000	100	350	6.0	0.40	[83]
Ni ₁ Co ₉ /CZY	10.0	23.6	6000	100	350	10.5	0.70	
20Ni/MS	20.0	20.0	30,000	100	650	95.1	31.84	
30Ni/MS	22.0	30.0	30,000	100	650	94.8	31.74	[84]
Ni-50/ATP	5.8	38.6	30,000	100	650	89.9	9.03	[85]

Table 2. Cont.

Catalyst	Metal Loading (wt.%)	S _{BET} (m ² g ⁻¹)	GHSV (mL·g _{cat} ⁻¹ ·h ⁻¹)	NH ₃ Inlet Flow (%)	T (°C)	NH ₃ Conversion (%)	H ₂ Formation Rate (mmol H ₂ g _{cat} ⁻¹ min ⁻¹)	Ref.
Co-Mg ₃ N ₂	5.4	12.0	36,000	100	500	15.0	6.03	
Co-CaNH	5.2	34.5	36,000	100	500	38.0	15.27	[86]
Co-BaNH	4.8	11.8	36,000	100	500	50.0	20.09	
100Co	-	25.0	18,000	100	550	18.0	3.62	[87]
NiO	-	25.0	18,000	100	550	3.0	0.60	[88]
NiO	-	18.7	12,000	100	500	1.0	0.00	[89]
Fe@CF(5)	4.4	19.0	36,000	100	550	5.0	2.01	
Fe@CF(10)	8.0	19.6	36,000	100	550	7.0	2.81	
Fe@CF(15)	13.5	21.1	36,000	100	550	12.0	4.82	[90]
Mo@CF(10)	7.0	19.7	36,000	100	550	3.0	1.21	
Mo@CF(15)	12.5	22.7	36,000	100	550	4.0	1.61	
CoMo-Ar-R	-	21.0	36,000	100	650	71.2	28.61	
CoMo-Air-R	-	23.7	36,000	100	650	73.4	29.49	[91]
Cs-Co ₃ Mo ₃ N	-	8.2	6000	100	450	48.0	3.21	[92]
Co ₃ Mo ₃ N	-	6.1	6000	100	450	30.0	2.01	
Ni ₃ Mo ₃ N	-	2.2	6000	100	450	18.0	1.21	[93]
Fe ₃ Mo ₃ N	-	8.8	6000	100	450	16.0	1.07	

In other work, $\text{Co}_3\text{Mo}_3\text{N}$, $\text{Ni}_3\text{Mo}_3\text{N}$ and $\text{Fe}_3\text{Mo}_3\text{N}$ were successfully prepared by temperature-programmed reaction of the corresponding oxide precursors with ammonia [93]. In spite of the small surface area ($<10 \text{ m}^2 \text{ g}^{-1}$) and large crystallite size ($>10 \text{ nm}$) generated, these materials showed a suitable performance in the ammonia decomposition reaction. Three catalysts exhibited an ammonia conversion of $>50\%$ at $550 \text{ }^\circ\text{C}$, and $\text{Co}_3\text{Mo}_3\text{N}$ was the catalyst that presented the lowest apparent activation energy ($E_a = 70.0 \text{ kJ mol}^{-1}$). As mentioned above, $\text{Co}_3\text{Mo}_3\text{N}$ had an adequate N binding energy, justifying this behavior.

Therefore, a high surface area is usually thought to be a positive factor for dispersing metals, resulting in a larger number of active sites and assisting the mass transfer of the reaction [14,31,34,55,76,94]. In contrast, it is found that the utilization of precursors, mainly perovskites or hydrotalcites, could help to control the metal size to be small, providing high dispersion. In addition, the oxygen vacancies improve the electronic state of the metal active phase as well as the metal–support interaction, preferred by lower electronegative elements. Another factor that might reduce the reaction temperature is the application of carbide species, such as the novel SiC, Fe_2C and Mo_2C . All of them allow the development of suitable catalysts with small surface areas but suitable catalytic properties for the generation of hydrogen from ammonia.

5. Conclusions and Future Prospects

Thermal decomposition of ammonia is an efficient technology for generating CO_x -free hydrogen, and it is established as an important factor in the development of ammonia as a “hydrogen carrier”. The design of an active catalyst to reduce the reaction temperature is one of the central pillars of this technology. However, the catalytic activity is influenced not only by the metal active phase, but also by the support, the addition of promoters and the synthesis method. Although the high-surface-area supports improve the metal dispersion, this review provides a current perception of materials with small surface area. These materials show attractive results in hydrogen production from ammonia. The modification of the chemical and morphological properties of the active phase with basic and conductive supports led to a suitable performance, despite their low porosity.

On the other hand, the utilization of precursors seems to be an original strategy to develop catalysts with small particle sizes, yielding an excellent ammonia conversion at low temperatures. Additionally, chemical elements with smaller electronegativity are preferred to enhance the activity and increase reaction kinetics favoring the rate-determining step.

The use of non-noble-metal catalysts and low-cost and eco-friendly supports could decrease the operation cost and reduce the reaction temperature, as well as increase the sustainability of the process. In addition, the utilization of other non-noble metals, different from nickel, cobalt, molybdenum and iron, must be further investigated. The synthesis method should be optimized to reduce the time and cost, taking into account the importance of the sustainability of the process. In situ characterization techniques could help to verify the difference in the catalytic surface, whereas operando methods will assist in understanding the behavior of the catalysts during the ammonia decomposition reaction.

The utilization of carbide materials such as SiC or MoC as catalytic supports for the ammonia decomposition reaction should be explored and studied. Additionally, ABO_3 formulations might enhance the ammonia conversion at low reaction temperatures. The different combinations of mono- and bimetallic perovskite-type oxides could promote the development of ammonia decomposition catalysts.

Author Contributions: M.P.: Investigation, Methodology, Validation, Visualization and Writing—Original Draft Preparation. P.S., A.R.d.I.O., A.R. and A.d.L.-C.: Conceptualization, Visualization, Writing—Reviewing, Supervision and Funding Acquisition. All authors have read and agreed to the published version of the manuscript.

Funding: This work was funded by the “Junta de Comunidades de Castilla-La Mancha (JCCM)” and European Union (FEDER funds SBPLY/21/180501/000165) and the University of Castilla-La Mancha (2022-PRED-20658).

Data Availability Statement: Not applicable.

Acknowledgments: The authors thank the “Junta de Comunidades de Castilla-La Mancha (JCCM)” and European Union (FEDER funds SBPLY/21/180501/000165). M. Pinzón thanks the University of Castilla-La Mancha for the predoctoral contract within the framework of the Plan Propio I+D+I (2022-PRED-20658).

Conflicts of Interest: The authors declare no conflict of interest.

References

1. Madurai Elavarasan, R.; Pugazhendhi, R.; Irfan, M.; Mihet-Popa, L.; Khan, I.A.; Campana, P.E. State-of-the-Art Sustainable Approaches for Deeper Decarbonization in Europe—An Endowment to Climate Neutral Vision. *Renew. Sustain. Energy Rev.* **2022**, *159*, 112204. [[CrossRef](#)]
2. Liu, Z.; Deng, Z.; He, G.; Wang, H.; Zhang, X.; Lin, J.; Qi, Y.; Liang, X. Challenges and Opportunities for Carbon Neutrality in China. *Nat. Rev. Earth Environ.* **2022**, *3*, 141–155. [[CrossRef](#)]
3. Capurso, T.; Stefanizzi, M.; Torresi, M.; Camporeale, S.M. Perspective of the Role of Hydrogen in the 21st Century Energy Transition. *Energy Convers. Manag.* **2022**, *251*, 114898. [[CrossRef](#)]
4. Niaz, S.; Manzoor, T.; Pandith, A.H. Hydrogen Storage: Materials, Methods and Perspectives. *Renew. Sustain. Energy Rev.* **2015**, *50*, 457–469. [[CrossRef](#)]
5. Bockris, J.O.; Veziroglu, T.N. A Solar-Hydrogen Energy System for Environmental Compatibility. *Environ. Conserv.* **1985**, *12*, 105–118. [[CrossRef](#)]
6. Osman, A.I.; Mehta, N.; Elgarahy, A.M.; Hefny, M.; Al-Hinai, A.; Al-Muhtaseb, H.A.; Rooney, D.W. Hydrogen Production, Storage, Utilisation and Environmental Impacts: A Review. *Environ. Chem. Lett.* **2022**, *20*, 153–188. [[CrossRef](#)]
7. Kapdan, I.K.; Kargi, F. Bio-Hydrogen Production from Waste Materials. *Enzym. Microb. Technol.* **2006**, *38*, 569–582. [[CrossRef](#)]
8. Bockris, J.O.M. The Hydrogen Economy: Its History. *Int. J. Hydrogphys. Energy* **2013**, *38*, 2579–2588. [[CrossRef](#)]
9. Hosseini, S.E.; Wahid, M.A. Hydrogen Production from Renewable and Sustainable Energy Resources: Promising Green Energy Carrier for Clean Development. *Renew. Sustain. Energy Rev.* **2016**, *57*, 850–866. [[CrossRef](#)]
10. Bassani, A.; Previtali, D.; Pirola, C.; Bozzano, G.; Colombo, S.; Manenti, F. Mitigating Carbon Dioxide Impact of Industrial Steam Methane Reformers by Acid Gas to Syngas Technology: Technical and Environmental Feasibility. *J. Sustain. Dev. Energy Water Environ. Syst.* **2020**, *8*, 71–87. [[CrossRef](#)]
11. Dawood, F.; Anda, M.; Shafiullah, G.M. Hydrogen Production for Energy: An Overview. *Int. J. Hydrogphys. Energy* **2020**, *45*, 3847–3869. [[CrossRef](#)]
12. Pawelczyk, E.; Łukasik, N.; Wysocka, I.; Rogala, A.; Gębicki, J. Recent Progress on Hydrogen Storage and Production Using Chemical Hydrogen Carriers. *Energies* **2022**, *15*, 4964. [[CrossRef](#)]
13. Zheng, J.; Zhou, H.; Wang, C.G.; Ye, E.; Xu, J.W.; Loh, X.J.; Li, Z. Current Research Progress and Perspectives on Liquid Hydrogen Rich Molecules in Sustainable Hydrogen Storage. *Energy Storage Mater.* **2021**, *35*, 695–722. [[CrossRef](#)]
14. Lucentini, I.; Garcia, X.; Vendrell, X.; Llorca, J. Review of the Decomposition of Ammonia to Generate Hydrogen. *Ind. Eng. Chem. Res.* **2021**, *60*, 18560–18611. [[CrossRef](#)]
15. Lamb, K.E.; Dolan, M.D.; Kennedy, D.F. Ammonia for Hydrogen Storage; A Review of Catalytic Ammonia Decomposition and Hydrogen Separation and Purification. *Int. J. Hydrogphys. Energy* **2019**, *44*, 3580–3593. [[CrossRef](#)]
16. Cesaro, Z.; Ives, M.; Nayak-Luke, R.; Mason, M.; Bañares-Alcántara, R. Ammonia to Power: Forecasting the Levelized Cost of Electricity from Green Ammonia in Large-Scale Power Plants. *Appl. Energy* **2021**, *282*, 116009. [[CrossRef](#)]
17. Ristig, S.; Poschmann, M.; Folke, J.; Gómez-Cápiro, O.; Chen, Z.; Sanchez-Bastardo, N.; Schlögl, R.; Heumann, S.; Ruland, H. Ammonia Decomposition in the Process Chain for a Renewable Hydrogen Supply. *Chem. Ing. Tech.* **2022**, *94*, 1413–1425. [[CrossRef](#)]
18. Chehade, G.; Dincer, I. Progress in Green Ammonia Production as Potential Carbon-Free Fuel. *Fuel* **2021**, *299*, 120845. [[CrossRef](#)]
19. Valera-Medina, A.; Amer-Hatem, F.; Azad, A.K.; Dedoussi, I.C.; De Joannon, M.; Fernandes, R.X.; Glarborg, P.; Hashemi, H.; He, X.; Mashruk, S.; et al. Review on Ammonia as a Potential Fuel: From Synthesis to Economics. *Energy Fuels* **2021**, *35*, 6964–7029. [[CrossRef](#)]
20. Aziz, M.; TriWijayanta, A.; Nandiyanto, A.B.D. Ammonia as Effective Hydrogen Storage: A Review on Production, Storage and Utilization. *Energies* **2020**, *13*, 3062. [[CrossRef](#)]
21. Arnaiz del Pozo, C.; Cloete, S. Techno-Economic Assessment of Blue and Green Ammonia as Energy Carriers in a Low-Carbon Future. *Energy Convers. Manag.* **2022**, *255*, 115312. [[CrossRef](#)]
22. Morlanés, N.; Katikaneni, S.P.; Paglieri, S.N.; Harale, A.; Solami, B.; Sarathy, S.M.; Gascon, J. A Technological Roadmap to the Ammonia Energy Economy: Current State and Missing Technologies. *Chem. Eng. J.* **2021**, *408*, 127310. [[CrossRef](#)]

23. Wan, Z.; Tao, Y.; Shao, J.; Zhang, Y.; You, H. Ammonia as an Effective Hydrogen Carrier and a Clean Fuel for Solid Oxide Fuel Cells. *Energy Convers. Manag.* **2021**, *228*, 113729. [CrossRef]
24. López-Fernández, E.; Sacedón, C.G.; Gil-Rostra, J.; Yubero, F.; González-Elipse, A.R.; de Lucas-Consuegra, A. Recent Advances in Alkaline Exchange Membrane Water Electrolysis and Electrode Manufacturing. *Molecules* **2021**, *26*, 6326. [CrossRef]
25. Barisano, D.; Canneto, G.; Nanna, F.; Villone, A.; Fanelli, E.; Freda, C.; Grieco, M.; Lotierzo, A.; Cornacchia, G.; Braccio, G.; et al. Investigation of an Intensified Thermo-Chemical Experimental Set-Up for Hydrogen Production from Biomass: Gasification Process Integrated to a Portable Purification System—Part II. *Energies* **2022**, *15*, 4580. [CrossRef]
26. Mutch, G.A. Electrochemical Separation Processes for Future Societal Challenges. *Cell Rep. Phys. Sci.* **2022**, *3*, 100844. [CrossRef]
27. Smith, C.; Hill, A.K.; Torrente-Murciano, L. Current and Future Role of Haber-Bosch Ammonia in a Carbon-Free Energy Landscape. *Energy Environ. Sci.* **2020**, *13*, 331–344. [CrossRef]
28. Soloveichik, G. Electrochemical Synthesis of Ammonia as a Potential Alternative to the Haber–Bosch Process. *Nat. Catal.* **2019**, *2*, 377–380. [CrossRef]
29. International Energy Agency. The Future of Hydrogen—Analysis-IEA. Available online: <https://www.iea.org/reports/the-future-of-hydrogen> (accessed on 3 November 2021).
30. Ciucci, M. Energy Policy: General Principles | Fact Sheets on the European Union. Available online: <https://www.europarl.europa.eu/factsheets/en/sheet/68/energy-policy-general-principles> (accessed on 26 July 2022).
31. Mateti, S.; Saranya, L.; Sathikumar, G.; Cai, Q.; Yao, Y.; Chen, Y.I. Nanomaterials Enhancing the Solid-State Storage and Decomposition of Ammonia. *Nanotechnology* **2022**, *33*, 222001. [CrossRef]
32. García-Bordejé, E.; Armenise, S.; Roldán, L. Toward Practical Application Of H₂ Generation From Ammonia Decomposition Guided by Rational Catalyst Design. *Catal. Rev.* **2014**, *56*, 220–237. [CrossRef]
33. Armenise, S.; García-Bordejé, E.; Valverde, J.L.; Romeo, E.; Monzón, A. A Langmuir–Hinshelwood Approach to the Kinetic Modelling of Catalytic Ammonia Decomposition in an Integral Reactor. *Phys. Chem. Chem. Phys.* **2013**, *15*, 12104. [CrossRef] [PubMed]
34. Le, T.A.; Do, Q.C.; Kim, Y.; Kim, T.W.; Chae, H.J. A Review on the Recent Developments of Ruthenium and Nickel Catalysts for CO_x-Free H₂ Generation by Ammonia Decomposition. *Korean J. Chem. Eng.* **2021**, *38*, 1087–1103. [CrossRef]
35. Ganley, J.C.; Thomas, F.S.; Seebauer, E.G.; Masel, R.I. A Priori Catalytic Activity Correlations: The Difficult Case of Hydrogen Production from Ammonia. *Catal. Lett.* **2004**, *96*, 117–122. [CrossRef]
36. Chellappa, A.S.; Fischer, C.M.; Thomson, W.J. Ammonia Decomposition Kinetics over Ni-Pt/Al₂O₃ for PEM Fuel Cell Applications. *Appl. Catal. A Gen.* **2002**, *227*, 231–240. [CrossRef]
37. BOISEN, A.; DAHL, S.; NORSKOV, J.; CHRISTENSEN, C. Why the Optimal Ammonia Synthesis Catalyst Is Not the Optimal Ammonia Decomposition Catalyst. *J. Catal.* **2005**, *230*, 309–312. [CrossRef]
38. García-García, F.R.; Guerrero-Ruiz, A.; Rodríguez-Ramos, I. Role of B5-Type Sites in Ru Catalysts Used for the NH₃ Decomposition Reaction. *Top. Catal.* **2009**, *52*, 758–764. [CrossRef]
39. Karim, A.M.; Prasad, V.; Mpourmpakis, G.; Lonergan, W.W.; Frenkel, A.I.; Chen, J.G.; Vlachos, D.G. Correlating Particle Size and Shape of Supported Ru/ γ -Al₂O₃ Catalysts with NH₃ Decomposition Activity. *J. Am. Chem. Soc.* **2009**, *131*, 12230–12239. [CrossRef]
40. Pinzón, M.; Romero, A.; de Lucas Consuegra, A.; de la Osa, A.R.; Sánchez, P. Hydrogen Production by Ammonia Decomposition over Ruthenium Supported on SiC Catalyst. *J. Ind. Eng. Chem.* **2021**, *94*, 326–335. [CrossRef]
41. Pinzón, M.; Avilés-García, O.; de la Osa, A.R.; de Lucas-Consuegra, A.; Sánchez, P.; Romero, A. New Catalysts Based on Reduced Graphene Oxide for Hydrogen Production from Ammonia Decomposition. *Sustain. Chem. Pharm.* **2022**, *25*, 100615. [CrossRef]
42. Pinzón, M.; Romero, A.; de Lucas-Consuegra, A.; de la Osa, A.R.; Sánchez, P. CO_x-Free Hydrogen Production from Ammonia at Low Temperature Using Co/SiC Catalyst: Effect of Promoter. *Catal. Today* **2022**, *390–391*, 34–47. [CrossRef]
43. Pinzón, M.; Sánchez-Sánchez, A.; Sánchez, P.; de la Osa, A.R.; Romero, A. Ammonia as a Carrier for Hydrogen Production by Using Lanthanum Based Perovskites. *Energy Convers. Manag.* **2021**, *246*, 114681. [CrossRef]
44. Pinzón, M.; Sánchez-Sánchez, A.; Romero, A.; de la Osa, A.R.; Sánchez, P. Self-Combustion Ni and Co-Based Perovskites as Catalyst Precursors for Ammonia Decomposition. Effect of Ce and Mg Doping. *Fuel* **2022**, *323*, 124384. [CrossRef]
45. Li, Y.; Wen, J.; Ali, A.M.; Duan, M.; Zhu, W.; Zhang, H.; Chen, C.; Li, Y. Size Structure–Catalytic Performance Correlation of Supported Ni/MCF-17 Catalysts for CO_x-Free Hydrogen Production. *Chem. Commun.* **2018**, *54*, 6364–6367. [CrossRef] [PubMed]
46. Bell, T.E.; Ménard, H.; González Carballo, J.-M.; Tooze, R.; Torrente-Murciano, L. Hydrogen Production from Ammonia Decomposition Using Co/ γ -Al₂O₃ Catalysts—Insights into the Effect of Synthetic Method. *Int. J. Hydrog. Energy* **2020**, *45*, 27210–27220. [CrossRef]
47. Duan, X.; Qian, G.; Liu, Y.; Ji, J.; Zhou, X.; Chen, D.; Yuan, W. Structure Sensitivity of Ammonia Decomposition over Ni Catalysts: A Computational and Experimental Study. *Fuel Process. Technol.* **2013**, *108*, 112–117. [CrossRef]
48. Bell, T.E.; Torrente-Murciano, L. H₂ Production via Ammonia Decomposition Using Non-Noble Metal Catalysts: A Review. *Top. Catal.* **2016**, *59*, 1438–1457. [CrossRef]
49. Hu, X.-C.; Wang, W.-W.; Jin, Z.; Wang, X.; Si, R.; Jia, C.-J. Transition Metal Nanoparticles Supported La-Promoted MgO as Catalysts for Hydrogen Production via Catalytic Decomposition of Ammonia. *J. Energy Chem.* **2019**, *38*, 41–49. [CrossRef]
50. Im, Y.; Muroyama, H.; Matsui, T.; Eguchi, K. Ammonia Decomposition over Nickel Catalysts Supported on Alkaline Earth Metal Aluminate for H₂ Production. *Int. J. Hydrog. Energy* **2020**, *45*, 26979–26988. [CrossRef]

51. Zhao, Z.; Zou, H.; Lin, W. Effect of Rare Earth and Other Cationic Promoters on Properties of CoMoNx/CNTs Catalysts for Ammonia Decomposition. *J. Rare Earths* **2013**, *31*, 247–250. [[CrossRef](#)]
52. Zheng, W.; Zhang, J.; Ge, Q.; Xu, H.; Li, W. Effects of CeO₂ Addition on Ni/Al₂O₃ Catalysts for the Reaction of Ammonia Decomposition to Hydrogen. *Appl. Catal. B Environ.* **2008**, *80*, 98–105. [[CrossRef](#)]
53. Mukherjee, S.; Devaguptapu, S.V.; Sviripa, A.; Lund, C.R.F.; Wu, G. Low-Temperature Ammonia Decomposition Catalysts for Hydrogen Generation. *Appl. Catal. B Environ.* **2018**, *226*, 162–181. [[CrossRef](#)]
54. Sayas, S.; Morlanés, N.; Katikaneni, S.P.; Harale, A.; Solami, B.; Gascon, J. High Pressure Ammonia Decomposition on Ru-K/CaO Catalysts. *Catal. Sci. Technol.* **2020**, *10*, 5027–5035. [[CrossRef](#)]
55. Sun, S.; Jiang, Q.; Zhao, D.; Cao, T.; Sha, H.; Zhang, C.; Song, H.; Da, Z. Ammonia as Hydrogen Carrier: Advances in Ammonia Decomposition Catalysts for Promising Hydrogen Production. *Renew. Sustain. Energy Rev.* **2022**, *169*, 112918. [[CrossRef](#)]
56. Hu, Z.; Mahin, J.; Datta, S.; Bell, T.E.; Torrente-Murciano, L. Ru-Based Catalysts for H₂ Production from Ammonia: Effect of 1D Support. *Top. Catal.* **2019**, *62*, 1169–1177. [[CrossRef](#)]
57. Furusawa, T.; Kuribara, H.; Kimura, K.; Sato, T.; Itoh, N. Development of a Cs-Ru/CeO₂ Spherical Catalyst Prepared by Impregnation and Washing Processes for Low-Temperature Decomposition of NH₃: Characterization and Kinetic Analysis Results. *Ind. Eng. Chem. Res.* **2020**, *59*, 18460–18470. [[CrossRef](#)]
58. Huang, C.; Yu, Y.; Yang, J.; Yan, Y.; Wang, D.; Hu, F.; Wang, X.; Zhang, R.; Feng, G. Ru/La₂O₃ Catalyst for Ammonia Decomposition to Hydrogen. *Appl. Surf. Sci.* **2019**, *476*, 928–936. [[CrossRef](#)]
59. Im, Y.; Muroyama, H.; Matsui, T.; Eguchi, K. Investigation on Catalytic Performance and Desorption Behaviors of Ruthenium Catalysts Supported on Rare-Earth Oxides for NH₃ Decomposition. *Int. J. Hydrogphys. Energy* **2022**, *47*, 32543–32551. [[CrossRef](#)]
60. Feng, J.; Zhang, X.; Wang, J.; Ju, X.; Liu, L.; Chen, P. Applications of Rare Earth Oxides in Catalytic Ammonia Synthesis and Decomposition. *Catal. Sci. Technol.* **2021**, *11*, 6330–6343. [[CrossRef](#)]
61. Muroyama, H.; Matsui, T.; Eguchi, K. Production and Utilization of Hydrogen Carriers by Using Supported Nickel Catalysts. *J. Jpn. Pet. Inst.* **2021**, *64*, 123–131. [[CrossRef](#)]
62. Zhang, X.; Liu, L.; Feng, J.; Ju, X.; Wang, J.; He, T.; Chen, P. Metal-Support Interaction-Modulated Catalytic Activity of Ru Nanoparticles on Sm₂O₃ for Efficient Ammonia Decomposition. *Catal. Sci. Technol.* **2021**, *11*, 2915–2923. [[CrossRef](#)]
63. Le, T.A.; Kim, Y.; Kim, H.W.; Lee, S.U.; Kim, J.R.; Kim, T.W.; Lee, Y.J.; Chae, H.J. Ru-Supported Lanthania-Ceria Composite as an Efficient Catalyst for CO_x-Free H₂ Production from Ammonia Decomposition. *Appl. Catal. B Environ.* **2021**, *285*, 119831. [[CrossRef](#)]
64. Doh, H.; Kim, H.Y.; Kim, G.S.; Cha, J.; Park, H.S.; Ham, H.C.; Yoon, S.P.; Han, J.; Nam, S.W.; Song, K.H.; et al. Influence of Cation Substitutions Based on ABO₃ Perovskite Materials, Sr₁-XYxTi₁-YRu_yO_{3-δ}, on Ammonia Dehydrogenation. *ACS Sustain. Chem. Eng.* **2017**, *5*, 9370–9379. [[CrossRef](#)]
65. Cao, C.F.; Wu, K.; Zhou, C.; Yao, Y.H.; Luo, Y.; Chen, C.Q.; Lin, L.; Jiang, L. Electronic Metal-Support Interaction Enhanced Ammonia Decomposition Efficiency of Perovskite Oxide Supported Ruthenium. *Chem. Eng. Sci.* **2022**, *257*, 117719. [[CrossRef](#)]
66. Zhiqiang, F.; Ziqing, W.; Dexing, L.; Jianxin, L.; Lingzhi, Y.; Qin, W.; Zhong, W. Catalytic Ammonia Decomposition to CO_x-Free Hydrogen over Ruthenium Catalyst Supported on Alkali Silicates. *Fuel* **2022**, *326*, 125094. [[CrossRef](#)]
67. Zhao, J.; Xu, S.; Wu, H.; You, Z.; Deng, L.; Qiu, X. Metal-Support Interactions on Ru/CaAlO: X Catalysts Derived from Structural Reconstruction of Ca-Al Layered Double Hydroxides for Ammonia Decomposition. *Chem. Commun.* **2019**, *55*, 14410–14413. [[CrossRef](#)]
68. Wang, Z.; Qu, Y.; Shen, X.; Cai, Z. Ruthenium Catalyst Supported on Ba Modified ZrO₂ for Ammonia Decomposition to CO_x-Free Hydrogen. *Int. J. Hydrogphys. Energy* **2019**, *44*, 7300–7307. [[CrossRef](#)]
69. Hu, Z.; Mahin, J.; Torrente-Murciano, L. A MOF-Templated Approach for Designing Ruthenium-Cesium Catalysts for Hydrogen Generation from Ammonia. *Int. J. Hydrogphys. Energy* **2019**, *44*, 30108–30118. [[CrossRef](#)]
70. Miyamoto, M.; Hamajima, A.; Oumi, Y.; Uemiya, S. Effect of Basicity of Metal Doped ZrO₂ Supports on Hydrogen Production Reactions. *Int. J. Hydrogphys. Energy* **2018**, *43*, 730–738. [[CrossRef](#)]
71. Chung, D.B.; Kim, H.Y.; Jeon, M.; Lee, D.H.; Park, H.S.; Choi, S.H.; Nam, S.W.; Jang, S.C.; Park, J.H.; Lee, K.Y.; et al. Enhanced Ammonia Dehydrogenation over Ru/La(x)-Al₂O₃ (x = 0–50 Mol%): Structural and Electronic Effects of La Doping. *Int. J. Hydrogphys. Energy* **2017**, *42*, 1639–1647. [[CrossRef](#)]
72. Okura, K.; Okanishi, T.; Muroyama, H.; Matsui, T.; Eguchi, K. Additive Effect of Alkaline Earth Metals on Ammonia Decomposition Reaction over Ni/Y₂O₃ Catalysts. *RSC Adv.* **2016**, *6*, 85142–85148. [[CrossRef](#)]
73. Yu, Y.; Gan, Y.; Huang, C.; Lu, Z.; Wang, X.; Zhang, R.; Feng, G. Ni/La₂O₃ and Ni/MgO–La₂O₃ Catalysts for the Decomposition of NH₃ into Hydrogen. *Int. J. Hydrogphys. Energy* **2020**, *45*, 16528–16539. [[CrossRef](#)]
74. Okura, K.; Okanishi, T.; Muroyama, H.; Matsui, T.; Eguchi, K. Ammonia Decomposition over Nickel Catalysts Supported on Rare-Earth Oxides for the On-Site Generation of Hydrogen. *ChemCatChem* **2016**, *8*, 2988–2995. [[CrossRef](#)]
75. Podila, S.; Driss, H.; Zaman, S.F.; Alhamed, Y.A.; Alzahrani, A.A.; Daous, M.A.; Petrov, L.A. Hydrogen Generation by Ammonia Decomposition Using Co/MgO–La₂O₃ Catalyst: Influence of Support Calcination Atmosphere. *J. Mol. Catal. A Chem.* **2016**, *414*, 130–139. [[CrossRef](#)]
76. Huang, C.; Yu, Y.; Tang, X.; Liu, Z.; Zhang, J.; Ye, C.; Ye, Y.; Zhang, R. Hydrogen Generation by Ammonia Decomposition over Co/CeO₂ Catalyst: Influence of Support Morphologies. *Appl. Surf. Sci.* **2020**, *532*, 147335. [[CrossRef](#)]

77. Okura, K.; Okanishi, T.; Muroyama, H.; Matsui, T.; Eguchi, K. Promotion Effect of Rare-Earth Elements on the Catalytic Decomposition of Ammonia over Ni/Al₂O₃ Catalyst. *Appl. Catal. A Gen.* **2015**, *505*, 77–85. [[CrossRef](#)]
78. Muroyama, H.; Saburi, C.; Matsui, T.; Eguchi, K. Ammonia Decomposition over Ni/La₂O₃ Catalyst for on-Site Generation of Hydrogen. *Appl. Catal. A Gen.* **2012**, *443–444*, 119–124. [[CrossRef](#)]
79. Podila, S.; Driss, H.; Ali, A.M.; Al-Zahrani, A.A.; Daous, M.A. Influence of Ce Substitution in LaMO₃ (M = Co/Ni) Perovskites for CO_x-Free Hydrogen Production from Ammonia Decomposition. *Arab. J. Chem.* **2022**, *15*, 103547. [[CrossRef](#)]
80. Al-attar, O.A.; Podila, S.; Al-Zahrani, A.A. Preparation and Study of XCeO₃ (X: Mg, Ca, Sr, Ba) Perovskite-Type Oxide Supported Cobalt Catalyst for Hydrogen Production by Ammonia Decomposition. *Arab. J. Sci. Eng.* **2022**, 1–11. [[CrossRef](#)]
81. Okura, K.; Miyazaki, K.; Muroyama, H.; Matsui, T.; Eguchi, K. Ammonia Decomposition over Ni Catalysts Supported on Perovskite-Type Oxides for the on-Site Generation of Hydrogen. *RSC Adv.* **2018**, *8*, 32102–32110. [[CrossRef](#)]
82. Zhao, J.; Deng, L.; Zheng, W.; Xu, S.; Yu, Q.; Qiu, X. Nickel-Induced Structure Transformation in Hydrocalumite for Enhanced Ammonia Decomposition. *Int. J. Hydrogphys. Energy* **2020**, *45*, 12244–12255. [[CrossRef](#)]
83. Huang, C.; Li, H.; Yang, J.; Wang, C.; Hu, F.; Wang, X.; Lu, Z.-H.; Feng, G.; Zhang, R. Ce_{0.6}Zr_{0.3}Y_{0.1}O₂ Solid Solutions-Supported Ni Co Bimetal Nanocatalysts for NH₃ Decomposition. *Appl. Surf. Sci.* **2019**, *478*, 708–716. [[CrossRef](#)]
84. Hu, Z.P.; Weng, C.C.; Yuan, G.G.; Lv, X.W.; Yuan, Z.Y. Ni Nanoparticles Supported on Mica for Efficient Decomposition of Ammonia to CO_x-Free Hydrogen. *Int. J. Hydrogphys. Energy* **2018**, *43*, 9663–9676. [[CrossRef](#)]
85. Li, L.; Chen, F.; Shao, J.; Dai, Y.; Ding, J.; Tang, Z. Attapulgitic Clay Supported Ni Nanoparticles Encapsulated by Porous Silica: Thermally Stable Catalysts for Ammonia Decomposition to CO_x Free Hydrogen. *Int. J. Hydrogphys. Energy* **2016**, *41*, 21157–21165. [[CrossRef](#)]
86. Yu, P.; Wu, H.; Guo, J.; Wang, P.; Chang, F.; Gao, W.; Zhang, W.; Liu, L.; Chen, P. Effect of BaNH, CaNH, Mg₃N₂ on the Activity of Co in NH₃ Decomposition Catalysis. *J. Energy Chem.* **2020**, *46*, 16–21. [[CrossRef](#)]
87. Zhang, Z.-S.; Fu, X.-P.; Wang, W.-W.; Jin, Z.; Song, Q.-S.; Jia, C.-J. Promoted Porous Co₃O₄-Al₂O₃ Catalysts for Ammonia Decomposition. *Sci. China Chem.* **2018**, *61*, 1389–1398. [[CrossRef](#)]
88. Yan, H.; Xu, Y.J.; Gu, Y.Q.; Li, H.; Wang, X.; Jin, Z.; Shi, S.; Si, R.; Jia, C.J.; Yan, C.H. Promoted Multimetal Oxide Catalysts for the Generation of Hydrogen via Ammonia Decomposition. *J. Phys. Chem. C* **2016**, *120*, 7685–7696. [[CrossRef](#)]
89. Nakamura, I.; Fujitani, T. Role of Metal Oxide Supports in NH₃ Decomposition over Ni Catalysts. *Appl. Catal. A Gen.* **2016**, *524*, 45–49. [[CrossRef](#)]
90. Guler, M.; Korkusuz, C.; Varisli, D. Catalytic Decomposition of Ammonia for Hydrogen Production over Carbon Nanofiber Supported Fe and Mo Catalysts in a Microwave Heated Reactor. *Int. J. Chem. React. Eng.* **2019**, *17*, 20180162. [[CrossRef](#)]
91. Duan, X.; Ji, J.; Yan, X.; Qian, G.; Chen, D.; Zhou, X. Understanding Co-Mo Catalyzed Ammonia Decomposition: Influence of Calcination Atmosphere and Identification of Active Phase. *ChemCatChem* **2016**, *8*, 938–945. [[CrossRef](#)]
92. Srifa, A.; Okura, K.; Okanishi, T.; Muroyama, H.; Matsui, T.; Eguchi, K. Hydrogen Production by Ammonia Decomposition over Cs-Modified Co₃Mo₃N Catalysts. *Appl. Catal. B Environ.* **2017**, *218*, 1–8. [[CrossRef](#)]
93. Srifa, A.; Okura, K.; Okanishi, T.; Muroyama, H.; Matsui, T.; Eguchi, K. CO_x-Free Hydrogen Production via Ammonia Decomposition over Molybdenum Nitride-Based Catalysts. *Catal. Sci. Technol.* **2016**, *6*, 7495–7504. [[CrossRef](#)]
94. Chen, C.; Wu, K.; Ren, H.; Zhou, C.; Luo, Y.; Lin, L.; Au, C.; Jiang, L. Ru-Based Catalysts for Ammonia Decomposition: A Mini-Review. *Energy Fuels* **2021**, *35*, 11693–11706. [[CrossRef](#)]